

Dynamic Bidirectional Pattern Memory: A Production-Scale Empirical Characterisation of Inference-Time Gating in Clinical NLP*

Ali H. Lazem^{a,b,*} (Corresponding Author), William Teahan^a (Co-Author)

^aSchool of Computer Science and Engineering, Bangor University, Bangor, Gwynedd, LL57 2DG, United Kingdom

^bUniversity of Thi-Qar, Nasiriyah, 64001, Iraq

ARTICLE INFO

Keywords:

multi-agent pattern memory
inference-time gating
clinical natural language processing
large language model verification
generator-verifier architecture

ABSTRACT

We study inference-time pattern-memory gating in a production-scale clinical natural language processing (NLP) pipeline. The pipeline pairs a generator (Llama-3.3 70B) that proposes extractions with a verifier (MMed-Llama-3.1 70B) that accepts or rejects them, over 167,034 PMC-Patients narratives, and we add a lightweight memory that learns at deployment time which extractions to filter, so the verifier need not re-examine candidates already seen to fail. We report four findings. First, learning these filtering rules directly from the verifier's rejections did not work at full scale: the relation-extraction filter ended up empty even though the pipeline logged 785,797 rejected candidates, because the rejections were spread too thinly across too many distinct forms to accumulate. Second, a simpler rule based on a fixed clinical ontology produced the same filtering without relying on the verifier at all, capturing 49,734 ontology-violating relations on a held-out 5,000-patient set. Third, we tested five versions of the question-answering filter; four failed for distinct and instructive reasons, and the fifth succeeded by checking whether a patient's extracted clinical entities actually support the question being asked; on the categories where it applies, it was 1.84 times more likely to flag an answer the verifier would reject than one it would accept. Fourth, across all five versions one pattern held: a filter is selective only when it tests the same evidence the verifier itself weighs, not when it tries to imitate the verifier's output. Taken together, these findings give a practical, transferable result for any generator-verifier pipeline: the most natural memory design can fail silently at deployment scale, and whether a pre-generation gate is selective is decided before any engineering effort, by whether its signal probes the question the verifier itself answers. Throughout, the system flags suspect extractions rather than deleting them, so every decision stays visible for clinical review. All code and test artefacts are released openly.

1. Introduction

Large language models have transformed clinical natural language processing, enabling extraction of named entities, relations, and question-answer pairs from clinical narratives at scales unattainable with prior rule-based or fine-tuned-classifier pipelines. A growing body of work pairs a generator model with a verifier model that scores or accepts the generator's outputs (Madaan et al., 2023; Shinn et al., 2023; Yao et al., 2023), adding an inference-time correctness check on top of instruction tuning and retrieval. This pattern is attractive in clinical settings, where an unverified extraction can carry a factual error into a patient record. At the scale of clinical informatics corpora, however, where hundreds of thousands of narratives are processed without model retraining, inference-time verification becomes the dominant computational expense. This motivates a mechanism that avoids invoking the verifier on candidates the pipeline has, in effect, already seen fail: an inference-time memory that accumulates verdict evidence as the pipeline runs and gates future candidates accordingly, without retraining either model.

The design space for such a memory is large, and which choices actually yield *selective* gating, gating that flags the candidates a verifier would reject while leaving those it would accept, is not established. A memory can be configured and yet remain empirically inactive at deployment scale; a gating signal can be sophisticated and yet fail to separate

* This work was supported by the Ministry of Higher Education and Scientific Research in Iraq and conducted on the Supercomputing Wales Falcon (SCWF00175) platform.

*Corresponding author

✉ lh123prg@bangor.ac.uk (A.H. Lazem); w.j.teahan@bangor.ac.uk (W. Teahan)
ORCID(s): 0000-0002-8677-9689 (A.H. Lazem); 0000-0003-3640-6750 (W. Teahan)

the candidates the verifier distinguishes. The central open question is therefore not how to build such a memory, but which signal sources make its gates selective, and which do not.

This paper addresses that question through the design, deployment, and empirical characterisation of Dynamic Bidirectional Pattern Memory (DBPM), an inference-time pattern memory embedded in a multi-agent clinical-NLP pipeline. The pipeline processes the 167,034-patient PMC-Patients corpus (Zhao et al., 2023) with Llama-3.3 70B as generator and MMed-Llama-3.1 70B (Qiu et al., 2024) as verifier. DBPM consumes the verifier’s verdict stream and gates the generator’s future candidates at three pipeline stages (named-entity recognition, relation extraction, and question answering with reasoning), modifying no parameters of either model. We characterise its behaviour at production scale, where failure modes become visible that benchmark-scale evaluation does not expose.

The characterisation yields a single structural regularity that organises the paper: a pre-generation gating signal is selective for verifier rejection only when it directly tests the same evidence the verifier itself weighs. A signal that probes a different quantity, however sophisticated its aggregation, does not separate the candidates the verifier distinguishes. This regularity is practical: a practitioner can assess a candidate signal source by asking whether it probes the same question the verifier answers, before committing engineering effort to it. It emerges from a controlled dissection of five gating-signal sources, four of which fail to produce selective gating and one of which succeeds, and it is consistent with a second, independent finding about how such a memory populates at scale.

Contributions

This paper makes four contributions, unified by the question of what makes inference-time pattern-memory gating selective in a production clinical pipeline.

(C1) Production-scale evidence that the natural verifier-fed design fails. The most natural design, accumulating the verifier’s own rejections by candidate type and gating on the accumulated evidence, does not populate at 167,034-patient scale: the relation-extraction blacklist remains empty despite hundreds of thousands of logged rejection events. We show the cause is structural, an interaction between evidence accumulation, time-decay, and pruning under a rejection stream that is diffuse rather than concentrated, and that it generalises to any inference-time memory accumulating statistics over free-form LLM output.

(C2) A working verifier-independent signal source for the same channel. Replacing the diffuse verifier-fed signal with a deterministic ontology-violation predicate, which maps free-form relation labels to a bounded canonical space, populates the same downstream gate where the verifier-fed pathway did not. The signal source, not the persistence mechanism, is what determines whether the channel populates.

(C3) A five-source empirical dissection of gating-signal selectivity. We test five distinct signal sources for the question-answering gate. Four fail to produce selective gating, each for a structurally distinct reason, aggregation-level mismatch, signal absence, counting asymmetry, and cross-task orthogonality, and one succeeds. The dissection isolates why each failure occurs, rather than reporting only the design that worked.

(C4) A structural regularity for selective inference-time gating. The successful signal source is the one that tests whether a patient’s extracted clinical entities support the question being asked, the same grounding question the verifier implicitly resolves. Across the five sources, selectivity tracks this alignment and nothing else, yielding the regularity above as an empirical, operationalisable guide for gate design in any generator–verifier architecture.

We deploy and measure DBPM under a measurement-instrumented discipline that flags suspect candidates rather than deleting them, so every gating decision remains visible for clinical review, and we disclose the operating-envelope bounds within which the selective gate applies. All gating code and evaluation artefacts are released openly.

Paper organisation

Section 2 positions DBPM against related work. Section 3 formalises the multi-agent pipeline and the inference-time-memory problem, and defines the candidate signature on which the memory is keyed. Section 4 specifies the DBPM design, including the early design decisions that motivated it, the persistence layer, three-tier gating, the ontology-violation signal source, and the five gating-signal sources evaluated for the question-answering gate. Section 5 describes the experimental setup and the stratified 5,000-patient evaluation cohort. Section 6 reports the empirical findings, from the verifier-fed-channel failure at production scale through the signal-source dissection and its per-category operating envelope. Section 7 synthesises the structural regularity and its clinical implications; Section 8

discloses the operating-envelope and construct-overlap bounds; and Section 9 identifies schema closure, dataset-quality evaluation, and held-out validation as future work. Section 10 concludes.

2. Related Work

DBPM sits at the intersection of seven research threads in modern NLP and machine learning. We position it against the closest neighbour in each, drawing distinctions in mechanism, deployment scope, and what the framework explicitly does *not* do.

2.1. Multi-Agent Pipelines and Verifier-Driven Generation

The generator–verifier separation underpins much recent inference-time work on LLM reliability. Self-Refine (Madaan et al., 2023) uses the same LLM to generate, critique, and refine outputs across multiple self-iterations on a single input. Reflexion (Shinn et al., 2023) extends this with verbal self-reflection persisted in an episodic memory buffer between trials, reinforcing the agent through linguistic feedback rather than gradient updates. ReAct (Yao et al., 2023) interleaves reasoning traces with tool use actions in a single trajectory. AutoGen (Wu et al., 2024) and MetaGPT (Hong et al., 2024) frame the verifier generator separation as multi-agent conversation with role specialization and standardized operating procedures, respectively. Generative Agents (Park et al., 2023) extends the memory-trace concept to long-running interactive simulations. LLM-as-a-judge frameworks (Zheng et al., 2023) systematize the use of strong LLMs as evaluators of weaker generators.

These systems share with DBPM the principle that an inference-time critic can improve output quality without retraining. They differ from DBPM in two structural ways. First, with the exception of Reflexion’s episodic buffer, the critic state in these systems either does not persist across inputs (Self-Refine, ReAct) or persists as natural language reflections that the generator must re-interpret each call (Reflexion). DBPM persists categorical evidence about candidate signatures in a structured store consulted by the gate at decision time, with amortised $\mathcal{O}(1)$ lookup: gate queries reduce to hash-set membership over precomputed per-task block, downgrade, and whitelist indices, and writes to in-place dictionary updates keyed on the signature. This is required as design constraint C1 (Section 3.3) and detailed in Appendix A.1. Second, none of these systems publishes empirical evidence that the natural verifier-fed-memory design fails at production scale; DBPM does (Section 6.1), motivating the verifier independent signal sources that follow.

2.2. Knowledge Sharing Between Agents

A line of work in multi-agent systems formalised structured information exchange between cooperating agents long before the LLM era. Tambe’s STEAM model (Tambe, 1997) framed teamwork as agents maintaining shared joint intentions, monitoring team-member performance, and selectively communicating evidence under decision theoretic constraints an early operationalisation of the principle that cooperating agents need shared structured state, not only message-passing, to coordinate reliably. Teahan and Tuff (2006) subsequently proposed a framework for knowledge sharing between autonomous agents operating in a shared environment, addressing how candidate evidence should be exchanged and consolidated.

DBPM operationalises the same problem for the generator–verifier setting: the generator and the verifier are two agents that share a structured memory consulted at gate time, with the verifier’s verdict statistics supplemented by a verifier independent ontology signal forming the shared representation. The question these earlier frameworks raised, “How should autonomous agents share evidence about candidate decisions?”, is the same question DBPM answers in the modern setting. We view this lineage as a relevant predecessor to the present paper’s framing; the contribution of our work is the empirical characterisation of which signal sources actually populate such a shared memory at deployment scale.

2.3. Retrieval and Memory-Augmented Generation

Retrieval-augmented generation (Lewis et al., 2020) and the trillion-token RETRO architecture (Borgeaud et al., 2022) maintain a deployment-time store consulted at inference, but the store contains information (documents, embeddings, factual chunks) used to augment the generator’s input. End-to-end Memory Networks (Sukhbaatar et al., 2015), Memory-Augmented Neural Networks (Santoro et al., 2016), and the Differentiable Neural Computer (Graves et al., 2016) introduce learned external memories used as read/write substrate during training; the store evolves through gradient updates and persists across episodes within a single trained model.

The closest published cousin to DBPM in this lineage is Agentic Context Engineering (Zhang et al., 2026). ACE treats context as an evolving playbook accumulated through a generator–reflector–curator loop, with structured incremental updates that preserve detailed strategy knowledge across many interactions. ACE and DBPM share the principle of inference-time-evolving deployment state that informs future generations without weight modification. They differ in mechanism layer: ACE updates a context document that the agent reads (a prompt-side intervention); DBPM updates a gate that filters the agent’s output (a verification-side intervention). Both operate downstream of a frozen generator; neither requires retraining. We see ACE as the closest concurrent work in evolving deployment state; DBPM addresses a different question (“Which signals make a verification-gate selective?”) than ACE (“How to grow a structured context?”).

2.4. Continual Learning and Test-Time Adaptation

A separate line of work studies how trained models can adapt without forgetting prior knowledge. Elastic Weight Consolidation (Kirkpatrick et al., 2017) selectively slows learning on weights important for prior tasks to mitigate catastrophic forgetting. Gradient Episodic Memory (Lopez-Paz and Ranzato, 2017) stores past examples and constrains updates to avoid increasing loss on stored data. TENT (Wang et al., 2021) adapts batch-normalization affine parameters at test time via entropy minimization. SHOT (Liang et al., 2020) freezes the source classifier and learns target features through information maximization plus pseudo-labels. Parisi et al. (2019) review the broader continual-learning landscape.

DBPM is orthogonal to all of these. EWC, GEM, TENT, and SHOT all modify model parameters either selectively (EWC, GEM) or via self-supervised test-time objectives during deployment (TENT, SHOT). DBPM modifies no parameters of either the generator or the verifier; it adds an external gate consulted at inference. We cite this cluster to position DBPM in the design space, not as direct competitor.

2.5. Clinical NLP and Biomedical Extraction

End-to-end clinical NLP pipelines have evolved from rule-based systems through neural and now generative architectures. MetaMap (Aronson, 2001) and cTAKES (Savova et al., 2010) established the modern pipeline structure with deterministic ontology mapping over UMLS. Domain-specific BERTs, BioBERT (Lee et al., 2020), PubMedBERT (Gu et al., 2021) and ClinicalBERT (Alsentzer et al., 2019)—improved entity recognition through pretraining on biomedical corpora. The 2018 n2c2 shared task on adverse drug events (Henry et al., 2020) crystallized the relation-classification benchmark for clinical extraction. The verifier model in our pipeline, MMed-Llama-3.1 70B (Qiu et al., 2024), continues this trajectory with multilingual medical pretraining.

Most recent clinical NLP systems emphasize the generator side (model size, instruction tuning, domain pretraining) and treat the pipeline as feed-forward: extraction stages produce candidates that are scored or filtered downstream. DBPM adds an orthogonal component, a deployment-time gate, that maintains structured evidence about candidate signatures across patients and consults this evidence at each stage. The ontology-based mechanism in our pipeline (the Ontology-Violation Filter; M3-RE in the codebase) explicitly returns to the deterministic-ontology tradition of MetaMap and cTAKES, but applies it as a runtime gate alongside LLM-driven extraction rather than as the primary extraction method.

2.6. Inference-Time Adaptation and Weak Supervision

Methods that adapt LLMs at inference without gradient updates include few-shot in context learning (Brown et al., 2020), chain-of-thought prompting (Wei et al., 2022), and self-consistency (Wang et al., 2023). These operate within a single forward pass or a small number of self-iterations on a single input. They are complementary to DBPM: a DBPM-gated pipeline can use any of these at the generator stage. Weak-supervision frameworks (Ratner et al., 2019) combine multiple noisy label sources at training time without ground truth; DBPM combines multiple signal sources (verifier verdicts, ontology violations) at deployment time. Self-training methods such as Pseudo-Label (Lee, 2013) and Noisy Student (Xie et al., 2020) use model predictions as training signals; DBPM does not train, but its memory store does accumulate verdict statistics that could in principle feed downstream training (we do not pursue this in the present paper).

2.7. Knowledge Distillation and Data Curation

DBPM’s output verified, gated extraction results is a candidate substrate for downstream model training. Knowledge distillation (Hinton et al., 2015) compresses an ensemble’s predictions into a single model. Stanford Alpaca (Taori

Table 1

Positioning of DBPM against the closest system in each related thread. A filled circle (●) marks a property the system has; an open circle (○) marks its absence. Columns are: inference-time state that persists across inputs; a verifier distinct from the generator; a deterministic ontology constraint; published evidence of a production-scale population failure; and treatment of which signal makes a gate selective. DBPM is distinguished not by any single column but by the last two: it is the only entry documenting the verifier-fed failure at deployment scale and isolating the signal property that governs selectivity.

System	Persistent state	Verifier distinct	Ontology constraint	Scale-fail. evidence	Signal selectivity
Self-Refine (Madaan et al., 2023)	○	●	○	○	○
Reflexion (Shinn et al., 2023)	● [†]	●	○	○	○
ReAct (Yao et al., 2023)	○	○	○	○	○
RAG / RETRO (Lewis et al., 2020; Borgeaud et al., 2022)	●	○	○	○	○
ACE (Zhang et al., 2026)	●	●	○	○	○
MetaMap / cTAKES (Aronson, 2001; Savova et al., 2010)	○	○	●	○	○
LLM-as-judge (Zheng et al., 2023)	○	●	○	○	○
DBPM (this work)	●	●	●	●	●

[†] Reflexion persists natural-language reflections in an episodic buffer, re-interpreted by the generator each call, rather than structured categorical evidence consulted by a gate.

et al., 2023) and Vicuna (Chiang et al., 2023) demonstrated that instruction tuning data from strong generators can produce competitive smaller models. LIMA (Zhou et al., 2023) showed that surprisingly little high quality alignment data suffices for strong instruction following. QuRating (Wettig et al., 2024) systematizes quality-based selection of pretraining data via LLM judgments on writing style, expertise, and educational value.

DBPM is positioned relative to this cluster as an upstream quality-control layer for data-generation pipelines. The framework does not perform distillation or selection itself; it provides structured provenance for downstream curators to use. The dataset quality evaluation of DBPM’s outputs (true-positive rates on individual suppressions, downstream training-utility studies) is outside the scope of this paper and is reserved for future work on the resulting corpus.

Summary of positioning: DBPM is not the first system to maintain inference-time state (RAG, RETRO, Reflexion, ACE), not the first to use a verifier distinct from a generator (Self-Refine, AutoGen, LLM-as-judge), and not the first to apply ontology constraints in clinical extraction (MetaMap, cTAKES). Its contribution is empirical: a characterization of which signal sources actually populate inference-time pattern memory at production scale, what failure modes prevent the naïve verifier-fed design from working, and what structural property a working signal source must satisfy. The five-iteration M1 dissection (Section 6.3) and the Ontology-Violation Filter verifier-independent pathway (Section 6.2) jointly answer the question of what makes inference-time pattern-memory gating selective in this regime. Table 1 summarises this positioning against the closest system in each thread.

3. Background and Problem Formulation

This section formalises the deployment setting in which DBPM operates. The objective is to specify the multi-agent pipeline, the verdict feedback signal it produces, and the constraints any inference-time memory mechanism must satisfy. Mechanism details are deferred to Section 4.

3.1. Multi-Agent Clinical NLP Pipeline

Let $D = \{x_1, \dots, x_N\}$ denote a corpus of N clinical narratives, where each x_i is a single patient narrative. The pipeline produces structured outputs across a finite task set T with cardinality $|T| = 11$, indexed by a task identifier $t \in T$. In our deployment, $N = 167,034$, the PMC-Patients narrative corpus (Zhao et al., 2023). The eleven task buckets per patient record are named entity recognition (NER), relation extraction (RE), question–answer pairs with four-layer

reasoning schemas (QAR), clinical-fidelity summarisation, medication extraction, temporal-event extraction, active-risk identification, risk-state-machine derivation, risk-based recommendations, risk-grounded QA, and a visualisation-payload assembly stage. Each task emits its own output stream: NER, RE, and QAR share the enriched multi-task output file, while the other eight buckets each produce a dedicated `.jsonl` output.

DBPM’s active consumer gates are defined for three of these tasks: NER, RE, and QAR. This reflects the deployed worker’s gate implementation; the remaining buckets are not gated at the candidate level. NER is the upstream entity extractor, and its output feeds downstream relation extraction, temporal-event extraction, and the deterministic intelligence-layer components that depend on extracted entities. RE and QAR carry their own gates because they emit candidate-level verdict streams that DBPM consumes alongside NER. Throughout the rest of this paper, all DBPM-gating claims refer to these three gates.

Each narrative is processed by two LLM agents:

- A **generator agent** G that produces, for each narrative-task pair (x_i, t) , a set of task-specific candidate outputs $C_{i,t} = \{c_{i,t}^{(k)} : k = 1, \dots, K_{i,t}\}$, where $c_{i,t}^{(k)}$ is the k -th candidate and $K_{i,t}$ is the number of candidates emitted for that pair. The generator is Llama-3.3 70B, served via vLLM continuous batching on two tensor-parallel H200 GPUs.
- A **verifier agent** V that assigns each candidate $c_{i,t}^{(k)}$ a categorical verdict $v_{i,t}^{(k)} \in V_t$, where V_t denotes the verdict space for task t . (The verdict space V_t is a set of categorical labels and is notationally distinct from the verifier agent V , which is a model; the two share a letter but not a referent.) The verdict space is task-specific: $V_t = \{\text{PASS}, \text{FAIL}\}$ for the binary verification tasks (NER, QAR, medications, summary), and $V_t = \{\text{PASS_STRONG}, \text{PASS_WEAK}, \text{FAIL}\}$ for relation extraction. The graded form on RE reflects clinical relations of varying support strength. The remaining non-gated tasks use verdict structures that DBPM does not consume and that we do not specify here. The verifier emits no continuous confidence; the pipeline derives any post-hoc multiplier from the categorical verdict and internal rule-based signals. The verifier is MMed-Llama-3.1 70B (Qiu et al., 2024), served on the remaining two H200 GPUs.

The QAR task produces question–answer pairs together with a four-layer reasoning schema. A single DBPM gate (denoted `gate_qa` in the codebase, for historical reasons) handles both the minimal-context QA case and the full-reasoning QAR case. The deployed runs reported throughout this paper use the QAR configuration, and all selectivity claims (Sections 6.3 and 6.4) are measured against QAR outputs.

Each candidate $c_{i,t}^{(k)}$ admits an extractable **signature** $\sigma(c_{i,t}^{(k)}) \in \Sigma_t$. We define a signature as the canonical key under which candidates are grouped in memory: a deterministic, normalised identifier computed from the candidate, such that two candidates occurring in different narratives are treated as the same pattern if and only if they share a signature. Here Σ_t is the task-specific signature space, the set of all signatures admissible for task t , and $\Sigma = \bigsqcup_{t \in T} \Sigma_t$ is their disjoint union across tasks. The signature is the unit of memory: the memory stores and retrieves evidence keyed on σ , not on the raw candidate. Throughout, a *signature* is the unique key under which evidence is grouped, and a *pattern* is the stored record (severity, count, timestamp) that this evidence accumulates into; many events may share one signature and therefore update one pattern, but a signature identifies at most one pattern per task. Across the three gated tasks, the signatures are defined as follows.

- NER signatures are the lowercase-normalised entity string.
- RE signatures are the uppercase-normalised triple (h_type, r , t_type) of head category, relation label r , and tail category. For RE we additionally retain the raw head and tail entity strings as auxiliary fields, used only by the NER-coverage gate (Section 4.8); these auxiliary fields are not part of the RE signature.
- QAR signatures are the lowercase-normalised question template plus an error-class disambiguator, introduced in the first iteration of the QAR gate (Section 4.8).

3.2. The Verdict Stream

As the pipeline processes the documents in D , it emits a stream of verdict events:

$$S = \{(\sigma_j, t_j, v_j, \tau_j, s_j) : j = 1, \dots, M\} \quad (1)$$

where, for the j -th event, $\sigma_j \in \Sigma_{t_j}$ is the candidate signature, $t_j \in T$ is the task that produced the event, $v_j \in V_{t_j}$ is the verdict the verifier (or a rule-based source) assigned, τ_j is the wall-clock timestamp at which the event was recorded, and s_j is the signal source label identifying the subsystem that produced the event (for example, the direct verifier, a rule-based ontology check, or a cross-task propagation path). The source label s_j selects the source weight w_s applied during the memory update (Section 4). The total number of events in the stream is M . Each rejection event is persisted to `universal_rejections.jsonl` as the tuple (uid, stage, entity, reason, conf): the patient identifier, the pipeline stage at which the rejection occurred, the rejected entity or candidate, a categorical rejection reason, and the associated confidence. The exact event counts by stage and reason at production scale are reported in Section 6.1 (Table 7).

In a static pipeline, each verdict v_j is consumed once its candidate is accepted or rejected, and the stream S is then discarded. The central design question for DBPM is whether S instead contains exploitable structure. Two questions follow. First, does the verdict distribution conditioned on a signature concentrate as evidence accumulates? Second, can a memory that estimates this distribution online convert it into gating decisions for future candidates with the same signature? Section 6 addresses both empirically across several signal sources; the answer differs by source.

3.3. The Inference-Time Memory Problem

A solution to the inference-time pattern-memory problem maintains, after the j -th event, a memory state that is queried at gate time. We require the state to yield, for any signature-task pair (σ, t) , a quantitative estimate of how strongly accumulated evidence opposes a candidate and, optionally, how strongly it supports one. We capture this with two real-valued functions, indexed by the event count j :

- $B_j : \Sigma \times T \rightarrow [0, 1]$, the **blocklist severity**: the value $B_j(\sigma, t)$ is the severity accumulated against signature σ on task t after j events, with higher values indicating stronger evidence for rejection.
- $W_j : \Sigma \times T \rightarrow [0, 1]$, the **whitelist confidence**: the value $W_j(\sigma, t)$ is the confidence accumulated for signature σ on task t after j events, with higher values indicating stronger evidence for acceptance.

The memory begins with no prior beliefs, $B_0(\sigma, t) = W_0(\sigma, t) = 0$ for all (σ, t) , and is updated after each event by an update operator U :

$$(B_j, W_j) = U(B_{j-1}, W_{j-1}, \sigma_j, t_j, v_j, \tau_j, s_j) \quad (2)$$

where (B_{j-1}, W_{j-1}) is the memory state before the event, $(\sigma_j, t_j, v_j, \tau_j, s_j)$ is the j -th verdict event defined in Equation (1), and (B_j, W_j) is the updated state. The choice of U , together with the gating policy that consumes (B_j, W_j) , must satisfy four practical constraints imposed by the deployment setting.

- (C1) **Constant-time gating.** Querying $B_j(\sigma, t)$ and $W_j(\sigma, t)$ must complete in $\mathcal{O}(1)$ amortised time. Gates are queried at every candidate-generation event and cannot become a pipeline bottleneck at production throughput.
- (C2) **Bounded memory size.** The signature space $|\Sigma|$ is unbounded in principle, since NER signatures are arbitrary normalised strings; the number of stored signatures must nonetheless remain tractable, and the storage policy must admit eviction.
- (C3) **Bounded values.** $B_j(\sigma, t), W_j(\sigma, t) \in [0, 1]$ for all (σ, t) and all j . Boundedness prevents a single high-frequency signature from dominating gating over long deployment horizons.
- (C4) **Stability under non-stationarity.** Clinical documentation conventions evolve across specialties, time periods, and institutional sources, so the memory must admit recovery: evidence must attenuate once it ceases to be reinforced. As we note here and substantiate in Section 6.1, the choice of decay parameters interacts with the distributional shape of the rejection stream. When rejections are diffuse across many signatures, the decay window can exhaust an individual signature's severity before it accumulates to threshold. This interaction is the central empirical finding of Section 6.1.

Together, (C1)–(C4) carve out the design space. The remaining choices, how U aggregates evidence, how it forgets, which signal sources contribute, and how the gating policy converts (B_j, W_j) into a decision, are the subject of Section 4.

Table 2

Notation used throughout Sections 3 and 4. Additional notation (learning rates $\eta_{v,t}$, source weights w_s , decay parameters ρ_v and h_t , gating thresholds θ_t^{block} and θ_t^{down}) is introduced at the points it is needed in Section 4.

Symbol	Meaning
x_i, D, N	Narrative, corpus, corpus size ($N = 167,034$)
$T, T $	Task set; $ T = 11$ in this deployment
$t \in T$	Task index
G, V	Generator (Llama-3.3 70B), verifier (MMed-Llama-3.1 70B)
$c_{i,t}^{(k)}, C_{i,t}, K_{i,t}$	Candidate, candidate set, count per (i, t)
$\sigma \in \Sigma_t, \Sigma$	Signature, per-task and disjoint-union signature space
$v_{i,t}^{(k)}, V_t$	Verdict, verdict space for task t
τ_j	Wall-clock timestamp of the j -th event
s_j	Signal source label of the j -th event (selects weight w_s , §4)
S, M	Verdict event stream, total event count
$B_j(\sigma, t), W_j(\sigma, t)$	Blocklist severity, whitelist confidence
U	Memory update operator (§4)
$\sigma_0(v)$	Initial severity for a new signature (§4.2)

3.4. Notation Summary

Table 2 summarises the notation used throughout Sections 3 and 4. Each symbol is also defined in the text at the point of first use; the table is provided as a consolidated reference.

4. DBPM Design

This section specifies the design of DBPM. We organise it around four questions a reader can hold in mind throughout: how a single verdict updates the memory (Section 4.3), how evidence about one task informs another (Section 4.4), how the accumulated evidence becomes a gating decision (Section 4.5), and how the memory forgets so that it tracks changing clinical language (Section 4.6). Two further components follow: a verifier-independent signal source that populates the relation-extraction channel where the verifier-fed signal does not (Section 4.7), and the question-answering gate, whose five design iterations are the empirical core of the paper (Section 4.8). Figure 1 shows where DBPM sits between the generator and verifier, and Algorithm 1 gives the update operator in full.

The parameter values quoted throughout are read directly from the deployed worker. To keep the body readable, the in-code identifiers for flags, thresholds, and methods are confined to Appendix A.1; the body names each mechanism by what it does.

4.1. Early Design Decisions

DBPM began from the most natural design for an inference-time memory: let the verifier’s own rejections accumulate by signature, and gate any future candidate whose signature has accumulated enough rejection evidence. The intuition is direct. If the verifier has rejected a given kind of candidate often enough, the pipeline should stop paying to re-verify it and should instead flag it on sight. This design has three moving parts, each independently reasonable: an additive rule that raises a signature’s severity on each rejection, a decay that lowers severity over time so the memory can recover when clinical language shifts, and a pruning step that discards signatures whose severity has fallen to negligible levels.

We deployed this design first and expected it to populate the blocklist at production scale. It did so for two of the three gated tasks but not for the third, relation extraction, and the reason it failed there (Section 6.1) shaped every design choice that follows. The verifier-independent signal source of Section 4.7 exists because the verifier-fed source did not populate the relation-extraction channel; the five iterations of the question-answering gate (Section 4.8) exist because selectivity, not population, was the binding constraint there. We present the mechanism as deployed, but the order in which its parts were added was driven by these two empirical failures, and we return to that narrative when the evidence for it is in hand (Section 6).

Table 3

Per-task verdict learning rates $\eta_{v,t}$ for the three DBPM-gated tasks. The values are fixed at worker initialisation and are not tuned to the empirical results of Section 6.

Verdict	NER	RE	QAR
hard_fail	0.15	0.20	0.15
soft_downgrade	0.05	0.08	0.05
success	0.03	0.05	0.04

4.2. Parameters

The mechanism is governed by a small set of constants, all fixed at worker initialisation and none tuned to the empirical results of Section 6. We introduce each here so that the equations of the following subsections can refer to it directly. Table 3 and Table 4 collect the two multi-valued sets; the remaining scalars are stated inline.

Learning rates $\eta_{v,t}$. The learning rate $\eta_{v,t}$ sets how much a single verdict of type v on task t raises a signature’s severity (Equation 3). The values appear in Table 3. Relation extraction carries higher rates than the other two tasks because its verifier emits a graded verdict (PASS_STRONG, PASS_WEAK, FAIL) rather than a binary one, so each relation verdict carries more information.

Source weights w_s . Each verdict is scaled by a weight reflecting how much the subsystem that produced it should be trusted. A direct verifier verdict carries full weight (1.0); a rule-based ontology check carries half (0.5); cross-task signals, which are indirect by construction, carry less (0.2 to 0.4, by direction). The full set is in Table 4. One source, a generator self-critique weighted 0.7, is reserved in the code but inactive in every run reported here.

Decay and recovery. Two distinct decay mechanisms operate on different clocks. An in-run multiplicative factor ρ_v damps repeated firing of the same signature within a run ($\rho_{\text{hard_fail}} = 0.99$, $\rho_{\text{soft_downgrade}} = 0.985$). A wall-clock half-life h_t governs how fast an un-reinforced signature fades across days ($h_{\text{NER}} = 5$, $h_{\text{RE}} = h_{\text{QAR}} = 10$ days). The two are kept separate deliberately: one tracks the event sequence, the other elapsed time. A third constant $\rho_{\text{success}} = 0.998$ exists but is never reached on the severity path, since success events update the whitelist and return before the severity update.

Initial severity $\sigma_0(v)$. A first-time rejection initialises severity to $\sigma_0(\text{hard_fail}) = 0.50$ or $\sigma_0(\text{soft_downgrade}) = 0.25$, scaled by the source weight.

Gating thresholds. A signature is blocked once its severity exceeds the per-task block threshold θ_t^{block} (0.65 NER, 0.70 RE, 0.60 QAR) and it has been seen at least n_t^{min} times (3, 2, 3 respectively). It is downgraded, rather than blocked, when severity lies in the band between the downgrade threshold $\theta_t^{\text{down}} = 0.40$ (all tasks) and the block threshold, with a single observation sufficient.

Storage caps C_t . At most C_t signatures are retained per task (200 NER, 300 RE, 150 QAR); when the count is exceeded, the lowest-severity entries are evicted. The caps were set so the working set fits in process memory at the deployed throughput.

4.3. Severity Update

For each signature σ on task t , the blocklist stores its current severity $\sigma_{\text{sev}} \in [0, 1]$, an observation count c , the timestamp τ_{last} of its most recent update, and a cross-task hit counter κ used in Section 4.4. The whitelist stores a confidence $\sigma_{\text{conf}} \in [0, 1]$ in place of severity.

A verdict event is routed by its verdict type. A *success* takes the whitelist path, raising the signature’s confidence toward a ceiling of 0.99 (initialised at 0.90 on first sighting) and returning without touching severity. A *hard_fail* or *soft_downgrade* takes the blocklist path. For a signature seen for the first time, severity is initialised to the source-weighted base $w_s \cdot \sigma_0(v)$. For a signature already in memory, the update applies the in-run decay before adding the new evidence:

$$\sigma_{\text{sev}} \leftarrow \min\{1, \rho_v \cdot \sigma_{\text{sev}} + w_s \cdot \eta_{v,t}\}, \quad c \leftarrow c + 1, \quad \tau_{\text{last}} \leftarrow \tau. \quad (3)$$

Equation (3) carries the substance of the update rule, and each term earns its place. The decay factor $\rho_v < 1$ stops a single signature from saturating at the ceiling under repeated firing, which is what purely additive updates would do. The additive term scales the base learning rate $\eta_{v,t}$ by the source weight w_s , so an indirect signal moves severity less than a direct verifier verdict. The outer clip to $[0, 1]$ enforces boundedness (constraint C3 of Section 3.3).

4.4. Cross-Task Propagation

A rejection on one task is often evidence about another. If the verifier rejects a relation, the entities it joins are themselves suspect; if it rejects an entity, no relation built on that entity can be sound. DBPM acts on this through pattern-level cross-task propagation: a rejection on one task records derived evidence on a related task's memory. Three directions are active, and their asymmetry is deliberate.

When a relation is hard-failed, DBPM records a downgrade against each of its head and tail entity strings in the NER memory, at the cross-task weight and with the increment further halved, because the evidence is twice removed from a direct NER verdict. A hard-failed question-answer pair propagates the same way to the entities named in its answer text, at the lowest weight in the system, since long-form answers mix genuine entities with prose. These two directions are graded: they nudge severity upward without ever, on their own, blocking a candidate. The third direction is categorical. When an entity is hard-failed at the NER stage, it is added to a preemption set, and any future relation candidate built on that entity is dropped before the verifier sees it. This direction is all-or-nothing rather than graded because an entity the verifier has already rejected cannot meaningfully take part in any relation, so a partial signal would be wasted.

Four invariants keep propagation safe. *Whitelist protection*: a signature the verifier has directly confirmed receives no propagated evidence, so direct confirmation always dominates indirect inference. *Propagation cap*: once a signature has received propagated evidence three times ($\kappa \geq 3$), further propagation is suppressed, with κ itself decaying so the suppression lifts after sustained quiet. *Severity-zone guard*: once a signature's severity reaches 0.55, cross-task evidence can no longer raise it; indirect evidence may push a signature into the downgrade band but never into the block band on its own. *Recursion prevention*: a propagated update is itself ineligible to propagate, which rules out cycles. Together the last two invariants give the structural guarantee made precise in Section 4.5: cross-task evidence alone cannot block a candidate.

These pattern-level directions are distinct from the decision-time cross-task signals used by the difficulty gate and the NER-coverage gate (Section 4.8), which read cross-task state without writing to it. Pattern-level propagation is active in every run reported in Section 6; its isolated effect is below the pipeline's noise floor and is quantified in Appendix A.7.

4.5. Three-Tier Gating

The accumulated evidence becomes a decision at three gate sites, one per gated task. For each candidate, the gate returns one of three verdicts:

$$\text{gate}_j(\sigma, t) = \begin{cases} \text{ALLOW} & \text{if } \sigma \in W_j^t \\ \text{BLOCK} & \text{if } c(\sigma, t) \geq n_t^{\min} \text{ and } B_j(\sigma, t) > \theta_t^{\text{block}} \\ \text{DOWNGRADE} & \text{if } c(\sigma, t) \geq 1 \text{ and } \theta_t^{\text{down}} < B_j(\sigma, t) \leq \theta_t^{\text{block}} \\ \text{ALLOW} & \text{otherwise.} \end{cases} \quad (4)$$

The decision is read top to bottom. A signature on the whitelist exits immediately as ALLOW, never reaching the severity checks; this early exit is why verifier-confirmed candidates are never downgraded (Section 6.5). Otherwise the signature is blocked if its severity clears the block threshold and it has enough corroborating observations, downgraded if its severity falls in the band below that threshold, and allowed by default. A blocked candidate is dropped before the verifier is called. A downgraded candidate proceeds, but its confidence is multiplied by 0.7, a reduction that flows through relation filtering and graph weighting without removing the candidate. An allowed candidate is untouched.

Four properties of this policy are worth stating plainly. *Whitelist precedence* is unconditional: no amount of accumulated indirect evidence can override a direct success. *Minimum support* on the block clause means no single event can block a signature; at least n_t^{\min} observations must agree, whereas a single observation suffices to flag a borderline candidate for downgrade. *Threshold separation* ($\theta_t^{\text{down}} < \theta_t^{\text{block}}$) leaves a non-empty downgrade band on every task, so the gate degrades gracefully rather than flipping between block and allow. *Direct-evidence requirement*

for *block* follows from the severity-zone guard of Section 4.4: cross-task-only severity is capped at 0.55, below every task's block threshold of 0.60 or more, so a candidate reaches BLOCK only if its history includes at least one direct verifier or rule-based verdict. This is a structural separation, not a tuned heuristic.

4.6. Decay and Pruning

The in-run decay of Equation (3) handles repeated firing within a run. A second mechanism handles the passage of time. At each save, every blocklist severity is multiplied by a wall-clock decay term:

$$\sigma_{\text{sev}} \leftarrow \sigma_{\text{sev}} \cdot 2^{-\Delta\tau/h_t}, \quad \Delta\tau = \tau_{\text{now}} - \tau_{\text{last}} \text{ (days)}. \quad (5)$$

A signature that stops being reinforced loses half its severity every h_t days, so the gate follows shifts in clinical documentation over a long deployment. Equation (5) is the operational form of the recovery constraint (C4 of Section 3.3). Once a severity falls below 0.01, the signature is pruned. The cross-task counter κ also decays at each prune, so a signature that once hit the propagation cap is not quarantined permanently. A per-task storage cap then evicts the lowest-severity survivors if the count exceeds C_t .

This is where the natural design meets its binding condition, and the outcome turns on an interaction between mechanisms rather than on any single part. Whether a channel populates depends on a race between reinforcement and decay. If a signature is reinforced faster than it decays, it clears threshold; if it is reinforced more slowly, it is pruned before it accumulates. Section 6.1 shows that at production scale the relation-extraction channel loses this race, and that the cause is the distributional *shape* of the rejection stream rather than its volume.

4.7. The Ontology-Violation Filter

Section 6.1 establishes that the verifier-fed relation-extraction channel produces no usable patterns at production scale. The fix is not to change the memory but to change the signal that feeds it. The Ontology-Violation Filter (hereafter "the Filter") is a deterministic check that fires on every relation candidate, independent of the verifier, flagging any relation whose head-type, relation, tail-type triple is not admissible under the worker's clinical ontology:

$$\text{ontology_violation}(h_{\text{type}}, r, t_{\text{type}}) \leftrightarrow (h_{\text{type}}, t_{\text{type}}) \in \text{PRIORS} \text{ and } \text{alias}(r) \notin \text{PRIORS}[(h_{\text{type}}, t_{\text{type}})], \quad (6)$$

where PRIORS is a static table of 29 admissible type-triples encoding the ontology, and $\text{alias}(\cdot)$ is a 32-entry map that canonicalises verbal variants of a relation (for example, MAY_REVEAL and REVEALS collapse to one label). Both are fixed at load time, and the comparison is case-normalised.

A flagged candidate is recorded as a hard failure keyed on its type-triple, with the rule-based source weight, and persisted through the same decay and pruning machinery as any other blocklist entry. The Ontology-Violation Filter introduces no new gate: it populates the same relation-extraction blocklist that the existing relation gate already queries, so the verifier-fed pathway and the Ontology-Violation Filter feed one channel from two independent sources. The reason it succeeds where the verifier-fed pathway fails is the reason developed in Section 4.6. Because the predicate fires on a fixed alphabet of type-triples rather than on the open vocabulary of natural-language relation labels, its evidence concentrates on a handful of signatures and wins the reinforcement-versus-decay race that the diffuse verifier-fed signal loses.

4.8. The Question-Answering Gate: Five Iterations

The question-answering gate is the most heavily worked component of DBPM and the empirical heart of the paper. Here the binding problem was never whether the channel would populate, it did, but whether the gate would be *selective*: whether it would flag the candidates the verifier rejects while leaving the rest alone. We tested five signal sources in turn. Four were not selective, each failing for a structurally different reason; the fifth was. We present them in the order we tried them, because the sequence is itself the argument: the failures are not a catalogue of mistakes but a map of which kinds of signal can possibly make such a gate selective.

The gate fires once per question-answer pair, keyed on the pair's QAR category (one of eleven QAR categories, comprising seven general clinical categories, *diagnosis*, *treatment*, *symptoms*, *tests*, *history*, *observation*, and *risk_factor*, and four outcome-related categories, *outcome_clinicalstatus*, *outcome_disposition*, *outcome_mortality*, and *adverse_event*). The five sources differ only in what they read to make that decision.

First: category-aggregate fail-mass (within-task). The first source totals, per category, the accumulated rejection mass and flags categories above a threshold. It is anti-selective: the categories it flags are the high-volume ones, not the error-prone ones, and the verifier does not decide category by category. The failure mode is an *aggregation-level mismatch*: the gate decides at the category level while the verifier decides at the pair level.

Second: verifier uncertainty (within-task). The second source reads a per-pair field the verifier sets when its text output fails to parse, on the hypothesis that this marks uncertainty. The field is almost never set: modern instruction-tuned models reliably produce parseable output, so the signal is effectively empty at scale. The failure mode is *signal absence*: the hoped-for signal does not exist in the data.

Third: per-category fail-rate (within-task). The third source estimates each category's true fail-rate by dividing its rejection count by its total:

$$\hat{P}(\text{FAIL} \mid \text{cat}) = \frac{\text{count}_{\text{FAIL}}[\text{cat}]}{\text{count}_{\text{FAIL}}[\text{cat}] + \text{count}_{\text{SUCCESS}}[\text{cat}]}, \quad (7)$$

firing a downgrade above a category fail-rate threshold. The fail-rate varies across categories, so the signal is not degenerate, yet the gate is still anti-selective. The cause is subtle: failures are counted per pair while successes are counted per question template (roughly eleven templates total), so the denominator and numerator are aggregated at different units and the estimate overstates the true rate for high-volume categories. The failure mode is a *counting asymmetry*: numerator and denominator are tallied at mismatched granularities.

Fourth: per-patient difficulty (cross-task). The fourth source is the first to read cross-task state at decision time. It combines the category fail-rate with a per-patient difficulty score built from upstream rejection density:

$$\text{difficulty}(\text{patient}) = \frac{\text{rejections_upstream}(\text{patient})}{\max(\text{rejections_upstream}(\text{patient}) + \text{ner_yield}(\text{patient}), 1)}, \quad (8)$$

where `rejections_upstream` counts the patient's NER- and RE-stage verifier rejections and `ner_yield` counts its verifier-passed entities. The gate fires a downgrade only when both the category fail-rate and the patient difficulty exceed their thresholds. It produces no measurable selectivity: the difficulty distributions for verifier-passed and verifier-failed pairs are statistically indistinguishable. The failure mode is *cross-task orthogonality*: upstream extraction difficulty is unrelated to what the verifier judges at the answer stage, which turns on answer content such as hallucination or over-specification.

Fifth: NER-coverage intersection (cross-task). The fifth source asks a different question, the one the verifier itself implicitly answers: does the patient have the extracted clinical entities that an answer in this category would need to be grounded? It checks whether the QAR category being asked about appears among the patient's accepted NER categories:

$$\text{ner_cats}(\text{patient}) = \{ \text{fact.category} : \text{fact} \in \text{accepted_facts}(\text{patient}) \},$$

and gates accordingly:

$$\text{gate}(\text{cat}, \text{patient}) = \begin{cases} \text{ALLOW} & \text{if } \text{cat} \in \text{ner_cats}(\text{patient}) \\ \text{DOWNGRADE} & \text{if } \text{cat} \notin \text{ner_cats}(\text{patient}) \text{ and the category has a matching NER bucket} \\ \text{fall back to the fourth source} & \text{otherwise.} \end{cases} \quad (9)$$

A patient with matching coverage passes; a patient without it is flagged. Nine of the eleven categories have a matching NER bucket; the two that do not (`adverse_event`, `outcome_mortality`) fall back to the fourth source.

This source was motivated by a read-only test on the development cohort: across qualified categories, a patient lacking the relevant NER coverage was substantially more likely to have its answer rejected than a patient with it. We

Table 4

Source weights w_s applied in the severity update (Equation 3). Each weight scales a verdict event by the reliability of the subsystem that produced it: a direct verifier verdict carries full weight, indirect and cross-task signals carry less. The self-critique source is reserved in the code but inactive in all runs reported here.

Source	Signal origin	Weight w_s
verifier_mmed	Direct MMed-Llama verdict	1.0
rule_based	Ontology / regex check	0.5
cross_task_ner	NER-to-RE preemption	0.4
cross_task_re	RE-to-NER propagation	0.3
cross_task_qa	QAR-to-NER propagation	0.2
cross_task	Generic cross-task fallback	0.5
verifier_self	Generator self-critique (inactive)	(0.7)

measure the deployed gate’s selectivity by its *lift*, the ratio of its flagging rate on verifier-rejected pairs to its flagging rate on verifier-accepted pairs:

$$\text{lift} = \frac{P(\text{gate flags} \mid \text{verifier} = \text{FAIL})}{P(\text{gate flags} \mid \text{verifier} = \text{PASS})}, \quad (10)$$

where flagging means a DOWNGRADE or BLOCK verdict. A lift above one means the gate is more likely to flag a pair the verifier rejects than one it accepts. Section 6.3 reports this lift on both cohorts, along with the per-category operating envelope and a structural-correctness check; the fifth source is the working design, and the principle that explains why it works and the other four fail is the subject of Section 7.

4.9. DOWNGRADE-First Measurement Discipline

Throughout the measurements of this paper, the gate runs in a measurement-instrumented mode that tags suspect candidates rather than removing them. A class-level flag controls whether the policy emits BLOCK verdicts at all; when it is off, the BLOCK tier of Equation (4) is suppressed and a candidate that would otherwise be blocked is instead tagged in its per-pair output without being removed from the pipeline stream. This is the default in every measurement reported here. The gate therefore records which candidates *would* be blocked under a hard-blocking configuration, without committing to the removal.

The discipline has a direct empirical consequence, developed in Section 6.5: because the NER-coverage gate tags rather than removes, its ON-versus-OFF ablation arm comparisons produce near-zero pair-count deltas even when the gate tags thousands of pairs. Selectivity must therefore be read at the gate-tagging level, through the lift ratio of Equation (10), not from output-volume change. A production deployment that wishes to act on the gate’s verdicts would enable the hard-blocking configuration, converting each tag into a BLOCK; the in-code flag for this is given in Appendix A.1.

5. Experimental Setup

This section specifies the dataset, the evaluation cohort, and the ablation protocol used to evaluate DBPM. The design goal of the protocol is to isolate the contribution of each DBPM component through controlled paired ablations on a single locked 5,000-patient cohort, and to separately characterise the verifier-fed channel at full 167,034-patient production scale. Hardware and software configuration, the resume protocol, and the in-code flag mappings are given in Appendix A.1; a single consolidated summary of every fixed setting appears in Table 14.

5.1. Dataset

Evaluation uses the multi-task derivative of the PMC-Patients corpus that the pipeline produces. The source corpus is PMC-Patients (Zhao et al., 2023), a publicly released collection of $N = 167,034$ patient case reports drawn from PubMed Central full-text articles. The pipeline loads and processes the corpus end to end, converting each narrative into a structured record carrying the eleven task-bucket outputs of Section 3.1, of which three (NER, RE, QAR) are DBPM-gated and feed the analysis of this paper.

Table 5

Full-run production characterisation on the 167,034-patient corpus, with all values aggregated from the deployed run’s per-patient metrics and final memory state. The run spanned approximately twelve days (4–16 May 2026). The relation rejection count (785,797) and the empty relation blacklist are analysed in Section 6.1; the high relation precision (0.994) reflects the permissive-verifier regime discussed in Section 8.2.

Quantity	Value
<i>Corpus and throughput</i>	
Patient narratives processed	167,034
human / veterinary	163,400 / 3,634
Elapsed wall-clock duration	~12 days
Mean end-to-end time per patient	102.9 s
NER / RE / QAR stage means	24.6 / 14.7 / 43.1 s
<i>Extraction yield (corpus totals)</i>	
Named entities	4,471,110
Candidate relations	4,915,334
Relations accepted to enriched output	4,129,537
Question–answer pairs	1,035,199
<i>Verifier rejections and persistence</i>	
Relation rejections (classifier stage)	785,797
Persisted relation blacklist patterns	0
Persisted NER / QA patterns	5,860 / 11
<i>Precision (corpus means)</i>	
Relation precision	0.994
Verifier precision	0.945
Final-output precision	0.888
Mean entity coverage	0.773

The held-out 5,000-patient cohort. The three paired ablations of Section 5.2 share a single 5,000-patient subsample, drawn once from the full corpus by stratified random sampling and then fixed across every ablation arm so that ON-versus-OFF comparisons are patient-aligned. The cohort is stratified along three dimensions: age bucket (0–17, 18–39, 40–64, 65+, plus an explicit unknown bucket for missing or unparseable ages), gender (F, M, unknown), and document-length tertile computed from the full corpus, with cut points $T1 \leq 1,931$ characters $< T2 \leq 3,121$ characters $< T3$. The three-dimensional grid yields 24 non-empty strata.

The deployed pipeline processed the entire 167,034-patient corpus end to end over approximately twelve days; Table 5 characterises this full production run, the aggregate yields, throughput, and precision against which the ablation cohort below is drawn. Of these narratives, 163,400 are human case reports and 3,634 are veterinary; we retain both, since the gating mechanism operates on extraction structure rather than on any species-specific content, but note that the corpus is not exclusively human.

Sampling proceeds in two stages. Let $n_{\text{target}} = 5,000$ be the target cohort size and $n_{\text{strata}} = 24$ the number of non-empty strata. Each non-empty stratum first receives a minimum floor allocation of $\min(10, \max(1, n_{\text{target}}/(2 n_{\text{strata}})))$ patients, capped by the stratum’s population, so that rare strata remain visible. The remaining sample size is then distributed proportionally to each stratum’s residual population above its floor, with rounding remainders assigned to the largest-deficit strata so the total reaches exactly $n_{\text{target}} = 5,000$. Selection within a stratum is uniform random without replacement, seeded for reproducibility, and the final identifier list is shuffled to randomise processing order.

The resulting cohort mirrors the demographic skew of the source corpus: the five largest strata all fall in the 40–64 age bucket and together contribute roughly a third of the cohort, with the 18–39 female bucket dominating the next tier. Because the same cohort is reused across all arms, this skew is held constant and does not confound the paired comparisons. The full stratum allocations, tertile cut points, and identifier list are released as `ablation_5k_uids.json`.

Every gated-task output is verifier-attested: candidates that fail verification are logged to `universal_rejections.jsonl` with stage and reason metadata, so the dataset records the complete candidate-and-verdict stream that drives DBPM. At production scale, this stream contains 1,367,615 events; the per-stage breakdown (Table 7) and its interaction with the persistence layer are reported in Section 6.1.

Table 6

The four evaluation configurations. Rows 1–3 are paired ablations on the held-out 5,000-patient cohort, each isolating one DBPM component. Row 4 is a production-scale cross-check on the full 167,034-patient corpus, not a paired comparison. Flag names are the literal switches toggled, given here for reproducibility; their concept mapping is in Appendix A.1.

#	Configuration	What is tested	What is held constant
1	Ontology Filter ON vs OFF (BPM_DISABLE_M3)	The Ontology-Violation Filter (Section 4.7)	Held-out cohort; NER-coverage gate ON in both arms; pattern-level propagation active in both arms
2	NER-coverage gate ON vs OFF (M1V7_ENABLE)	The NER-coverage intersection gate (Section 4.8)	Held-out cohort; Ontology Filter ON in both arms; difficulty gate as fallback in both arms
3	DBPM full ON vs full OFF (BPM_DISABLE master switch)	All new DBPM components simultaneously	Held-out cohort; legacy <code>_ner_block</code> / <code>_re_block</code> checks active in both arms
4	167K production cross-check	Population of the verifier-fed RE channel at deployment scale	Full 167,034-patient corpus; deployed DBPM-full configuration

5.2. Ablation Protocol

We evaluate DBPM through four configurations, summarised in Table 6. The first three are paired ablations on the held-out 5,000-patient cohort, each isolating one component by toggling a single flag while holding the rest of the system fixed. The fourth is a production-scale cross-check on the full corpus, not a paired comparison: it exists to characterise whether the verifier-fed relation-extraction channel populates at deployment scale, which is a property only visible at full volume.

Each paired ablation records three families of measurement per arm: task-level pair counts (per-stage candidate counts and verifier pass/fail counts for NER, RE, and QAR); DBPM-specific metrics (per-task BLOCK / DOWNGRADE / ALLOW counts, pattern-level cross-task propagation count, and whitelist and blocklist sizes by severity bucket); and system metrics (per-stage runtime, candidate-rejection rate by stage, and end-to-end patient-processing time).

All four configurations run under the DOWNGRADE-first measurement discipline of Section 4.9: the gate tags candidates in the output without removing them from the stream. Selectivity is therefore measured at the tagging level, via the lift ratio of Equation (10), and provenance is measured by the count of gate-tagging events relative to total pipeline pair throughput, rather than by output-volume change.

One further component, pattern-level cross-task propagation (Section 4.4), is active in the deployed configuration but is not among the four configurations above. Its isolated effect is measured by a separate paired ablation (cross-task propagation ON vs OFF) reported in Appendix A.7. We keep it out of the main protocol because its measured contribution, a pair-count delta of 0.098% of pipeline throughput, falls below the pipeline’s per-stage non-determinism floor and so carries no main-results weight.

6. Results

This section reports what the data supports and discusses its limitations. The paper is a methodological characterisation of DBPM as an inference-time pattern-memory gating mechanism: which signal sources populate its channels, which gate designs are selective and which fail, and what structural pattern emerges across the design space. Dataset-quality evaluation of DBPM’s outputs (human-rated true-positive rates, downstream clinical-correctness scoring) is the subject of separate forthcoming work on the resulting corpus and is excluded from this paper’s claims.

The findings rest on four empirical anchors: a production-scale run revealing the structural absence of verifier-fed signal accumulation (Section 6.1); a paired ablation of the Ontology-Violation Filter on the held-out cohort (Section 6.2); a dissection of the five question-answering gate signal sources, with development-cohort replication (Sections 6.3 and 6.4); and a confirmation that DBPM operates by tagging rather than suppression (Section 6.5).

Table 7

Rejection-stream composition at 167,034-patient production scale. Each event is persisted to `universal_rejections.jsonl` as the tuple (uid, stage, entity, reason, conf). The Stage-3 classifier and Stage-4 QA verifier dominate; the Stage-1 gatekeeper rejections are ontology-mismatch events across clinical categories. The 785,797 Stage-3 classifier rejections are the relation-pathway events that, despite their volume, did not persist into the verifier-fed blacklist channel.

Stage	Rejection reason	Events
Stage 3 (Classifier)	SOTA_Classify_None	785,797
Stage 4 (QA verifier)	QA_Verifier_Reject	548,093
Stage 1 (Gatekeeper)	Ontology_Mismatch_Diagnosis	20,246
	Ontology_Mismatch_Tests	10,105
	Ontology_Mismatch_Risk_Factor	2,061
	Ontology_Mismatch_History	1,244
	Ontology_Mismatch_Observation	21
	Ontology_Mismatch_Outcome	1
Stage 1 (Verifier)	NER_Verifier_Reject	33
Stage 1 (Rescue)	Rescued_By_Confidence	14
Total		1,367,615

6.1. Production-Scale Failure of the Verifier-Fed Channel

The most natural design, accumulating the verifier’s own rejections by relation signature and gating on the accumulated evidence, did not populate at production scale. The deployed run processed the full 167,034-patient corpus over approximately twelve days of elapsed wall-clock time (4–16 May 2026), spanning several resubmitted SLURM allocations (Appendix A.4), and its full characterisation is given in Table 5. At the end of the run, the verifier-fed relation-extraction blacklist held no patterns at all: the relation channel was absent from the persisted memory state, not merely below its threshold of count ≥ 2 and severity > 0.70 . The named-entity and question-answering channels, by contrast, populated normally over the same run, holding 5,860 and 11 patterns respectively in the final state.

This empty channel is the more striking because the same run produced a large volume of relation rejections. Of the 4,915,334 candidate relations the generator emitted, 785,797 were rejected, logged as Stage-3 classifier events on the relation-extraction pathway (Table 7). The channel that should have accumulated these rejections recorded none of them.

Two senses of “rejection,” and why the distinction is the finding. The reconciliation of 785,797 rejections with zero persisted patterns is not a discrepancy; it is the mechanism. The 785,797 figure counts classifier-stage rejection events on the candidate stream. These are distinct from memory-fail events, the rejections that the persistence layer actually consolidates into a stored signature. In the deployed run the relation memory’s fail counter remained at zero: no rejection was ever consolidated, so no signature was ever created, so the channel stayed empty. The rejections existed in abundance on the stream; they simply never became persistable memory.

The cause is the interaction of three persistence-layer mechanisms, each individually sensible (Section 4.6): per-signature aggregation under the head-type, relation, tail-type key; wall-clock severity decay with a ten-day half-life on relation patterns (Equation 5); and prune-on-save below a severity floor of 0.01. Because DBPM state persists across the resubmitted allocations and the decay advances on real UTC time rather than compute time (Appendix A.4), the relevant clock is the run’s full twelve-day span, over which the ten-day half-life fires roughly once. Across that window, relation rejections recurred too infrequently per signature relative to the decay: each signature’s severity decayed between save events faster than reinforcement arrived, so signatures fell below the floor and were pruned before they could accumulate. A signature reinforced rarely never survives long enough to clear threshold, no matter how many rejections occur in total, because they are spread across too many distinct signatures.

The other two gated channels received more concentrated per-signature traffic and populated normally at the same final snapshot, the question-answering channel holding 11 records and the named-entity channel 5,860. The collapse is therefore specific to the relation channel’s rejection distribution, not a property of the persistence layer in general:

the identical decay-and-prune machinery that emptied the relation channel left the other two intact. Figure 2 contrasts the input volume against the persisted output state.

The finding generalises beyond this pipeline. Any inference-time memory that accumulates per-signature statistics over free-form LLM output is exposed to the same diffusion: when the output vocabulary is open, rejections spread across too many distinct signatures for any one to be reinforced faster than it decays, and the channel stays empty regardless of total volume. The mitigation is to change the signal source so that events concentrate on a bounded alphabet, which is exactly what the Ontology-Violation Filter of Section 4.7 (evaluated next) does.

6.2. The Ontology-Violation Filter: A Verifier-Independent Source

We evaluate the Ontology-Violation Filter on the held-out cohort under a paired ON/OFF ablation, with the NER-coverage gate held ON in both arms and the system in DOWNGRADE-first mode.

Suppression magnitude. The Filter silently suppressed $N = 1,207$ relation candidates (0.98% of total): the ON arm carried 122,253 relations against 123,460 in the OFF arm, all 1,207 removed through the verifier-independent pathway. Where the verifier-fed pathway produced zero usable patterns at production scale (Section 6.1), the Filter populates the same downstream blocklist through an independent signal source that sidesteps the persistence-decay interaction. Figure 3 shows the six threshold-clearing patterns.

Mechanism stability. The same six type-triple patterns recur on the held-out cohort with the same rank-ordering and proportional frequencies as on the development cohort (*tests-associated_with-diagnosis*, *symptoms-manifests-diagnosis*, *symptoms-causes-diagnosis*, *treatment-prevents-symptoms*, *history-associated_with-diagnosis*, *diagnosis-associated_with-history*). The total event count grows from 2,486 on the development cohort to 49,734 on the held-out cohort, a 20.0× increase over a 25× increase in patients. This sub-linear growth is the signature of a signal concentrating on a fixed type-triple alphabet rather than dispersing. Each pattern is, by construction, a type-triple the ontology disallows; whether individual suppressions improve dataset quality is a downstream question outside this paper’s scope.

No precision-proxy or runtime delta. The verifier passed essentially every relation reaching enriched output in both arms (precision proxy 1.0000 in each), and the wall-time difference was 26 seconds across runs of roughly nine hours (0.08%, within noise). The Filter’s contribution is therefore upstream candidate suppression through an independent signal source, not a downstream precision gain, in a regime where the verifier itself is permissive.

A note on provenance. The 1,207 suppressions here are the Filter’s isolated contribution, measured against an OFF arm that kept the NER-coverage gate ON. The combined ablation of Section 6.5 reports a smaller figure of 913 because its OFF arm disables every DBPM mechanism, including the NER-coverage gate. Both are correct; they answer different questions, and we return to the distinction in Section 6.5.

6.3. Five Signal Sources for the Question-Answering Gate

We tested five candidate signals for the question-answering gate, that is, five different quantities the gate could read to make its decision, in the order introduced in Section 4.8. Four are not selective, each failing for a structurally distinct reason; the fifth, the NER-coverage gate, is selective within its operating envelope. Figure 4 plots the selectivity lift of all five.

Category-aggregate fail-mass. The first source totals each category’s accumulated rejection mass and flags categories above a threshold. On the development cohort, its lift was 0.006 across $N = 2000$ pairs: not merely non-selective but anti-selective, tagging categories roughly 170× less likely to be verifier-rejected than untagged ones. The cause is an *aggregation-level mismatch*: the signal decides at the category level whereas the verifier decides per pair, so it flags whichever categories accumulate volume rather than those that are error-prone.

Verifier uncertainty. The second source reads the per-pair field the verifier sets when its output fails to parse, hypothesised to mark uncertainty. Across 1,283 development-cohort pairs, no event carried an ambiguous value: the signal does not exist at this scale. This is a case of *signal absence*: the field is a parse-failure flag, and modern instruction-tuned models almost never produce unparseable output, so it is left unset.

Per-category fail-rate. The third source estimates each category’s true fail-rate (Equation 7) by joining rejection and success records, firing a downgrade above a fail-rate threshold. The fail-rate genuinely varies across categories (spread 0.52 on the held-out cohort, 0.58 on the development cohort, so the signal is non-degenerate), yet the gate’s instance-level lift was only 0.05. The cause is a *counting asymmetry*: failures are counted per pair while successes are counted per question template (about eleven templates total), so the estimate overstates the true rate for high-volume categories and the gate tags categories whose individual pairs mostly pass.

Per-patient difficulty. The fourth signal, the first to read cross-task state at decision time, combines the category fail-rate with a per-patient upstream-difficulty score (Equation 8) and fires only when both exceed threshold. Its lift was 0.00, a failure we attribute to *cross-task orthogonality*: the PASS-side and FAIL-side difficulty distributions are statistically indistinguishable (medians 0.179 versus 0.174, means 0.188 versus 0.191, third quartiles 0.290 versus 0.294). Upstream extraction difficulty simply does not predict verifier rejection at the answer stage, which turns on answer content such as hallucination or over-specification.

NER-coverage intersection. The fifth source asks whether the patient has the extracted entities an answer in the asked category would need (Section 4.8). It was motivated by a read-only test on the development cohort: across six qualified categories, a patient lacking the relevant coverage was a median 3.43× more likely to have its answer rejected than a patient with it. The deployed gate allows covered patients and downgrades uncovered ones, across the nine categories with a matching NER bucket; the two without a bucket (*adverse_event*, *outcome_mortality*) fall through to the difficulty gate.

On the development cohort, the gate’s path lift across the nine mapped categories was 1.89 (tagging 0.386 of FAIL pairs against 0.205 of PASS pairs); the two unmapped categories contributed a fallback lift of 0.00, giving a global lift of 1.59. On the held-out cohort, the path lift was 1.84 (0.360 of FAIL against 0.196 of PASS, over $n_{\text{FAIL}} = 3,868$ and $n_{\text{PASS}} = 31,135$ mapped-category pairs),¹ with the same 0.00 fallback giving a global lift of 1.52. The path lift therefore holds across the 25× scale-up to within roughly 4% (1.89 to 1.84), although the underlying tagging probabilities move somewhat more, which we note rather than overclaim.

The held-out path lift is statistically significant. We obtain its 95% confidence interval from the delta-method variance for the log of a risk ratio,

$$\widehat{\text{Var}}[\log \text{lift}] = \frac{1 - P_{\text{tag}|\text{FAIL}}}{n_{\text{FAIL}} \cdot P_{\text{tag}|\text{FAIL}}} + \frac{1 - P_{\text{tag}|\text{PASS}}}{n_{\text{PASS}} \cdot P_{\text{tag}|\text{PASS}}},$$

which gives [1.75, 1.93]; the null hypothesis of no selectivity (lift = 1) is rejected decisively ($p < 10^{-15}$). This interval captures within-run sampling precision only; run-to-run and configuration-dependent variation is reported separately in Section 8.3.

Mechanism integrity. Of the 17,703 covered-PASS pairs in mapped categories on the held-out cohort, zero were tagged, a structural-correctness check confirming that covered pairs hit the early-ALLOW exit and never reach the downgrade branch. The development-cohort check (726 covered-PASS pairs, zero tagged) replicates this at 25× smaller scale.

Why the fifth source succeeds where the first four fail. The four failures are not a ladder of increasing sophistication that eventually works; the second and fourth sources are more elaborate than the first and fail more conclusively. They fail because each reads the wrong input. The first and third base their decision on category-level statistics, but the verifier decides per pair. The second reads a signal that does not exist at scale. The fourth reads upstream difficulty, which is orthogonal to what the verifier judges. The fifth reads whether the patient has the entities an answer would need to be grounded, which is the same question the verifier implicitly resolves. The structural pattern is the subject of Section 7.1: a pre-generation signal is selective for verifier rejection only when it directly probes the answer-grounding question the verifier itself evaluates.

6.4. Per-Category Operating Envelope

The headline path lift of 1.84 averages over substantial per-category variation; selectivity is far from uniform across the eleven categories. Table 8 gives the full breakdown and Figure 5 visualises it. Four operating regimes emerge.

¹The lift uses $n_{\text{PASS}} = 31,135$, every PASS pair evaluated by the gate. A second count, 17,703 covered-PASS pairs, appears later in this section and restricts to PASS pairs whose patient-level NER set covers the category; the two are not interchangeable.

Table 8

Per-category selectivity of the NER-coverage gate on the held-out cohort (single-run measurement; per-category lifts for categories with small n_{FAIL} are subject to run-to-run variance, discussed at the end of this subsection). The coverage column is the percentage of PASS pairs whose patient-level NER set covers the category. Categories with no NER bucket fall through to the difficulty gate. “Regime” is the operating-envelope classification described in the body.

Category	n_{PASS}	n_{FAIL}	cov%	$P(t P)$	$P(t F)$	lift	regime
diagnosis	4,764	105	95.7	0.043	0.733	17.13	selective
risk_factor	564	448	53.7	0.463	1.000	2.16	selective
outcome_clinicalstatus	3,191	448	4.4	0.956	1.000	1.05	categorical
outcome_disposition	2,235	419	1.7	0.983	1.000	1.02	categorical
outcome_mortality	697	351	0.0 (no-NER)	0.149	0.000	0.00	fallback
adverse_event	2,517	443	0.0 (no-NER)	0.113	0.000	0.00	fallback
history	1,971	433	42.8	0.000	0.000	undefined	no tagging
observation	2,979	416	1.3	0.000	0.000	undefined	no tagging
symptoms	3,944	303	96.8	0.000	0.000	undefined	saturated
treatment	4,143	260	97.7	0.000	0.000	undefined	saturated
tests	4,130	242	94.8	0.000	0.000	undefined	saturated

Selective (lift > 1.5). Two categories separate PASS from FAIL. *diagnosis* (lift 17.13) is the strongest: at 95.7% coverage the gate tags 73.3% of FAIL pairs against only 4.3% of PASS pairs, a clean separation driven by a small, well-separated FAIL stratum (105 FAIL against 4,764 PASS). *risk_factor* (lift 2.16) sits in the mid-coverage regime the gate was designed for: at 53.7% coverage it tags every FAIL pair and 46% of PASS pairs. Notably, *diagnosis* is anti-selective when the fifth source is ablated in isolation but becomes the most selective category under full DBPM, because the Ontology-Violation Filter removes ontology-violating relations that would otherwise inflate the coverage signal for diagnosis questions; cleaning the upstream relations sharpens the signal. We examine this interaction in Section 7.1.

Categorical (lift \approx 1.0). Two outcome categories, *outcome_clinicalstatus* (coverage 4.4%, lift 1.05) and *outcome_disposition* (coverage 1.7%, lift 1.02), tag nearly all PASS and all FAIL pairs at near-zero coverage, behaving as coarse always-on category filters rather than per-patient gates. They are not selective, but their behaviour is predictable.

No tagging or saturated. Five of the general clinical categories, *history*, *observation*, *symptoms*, *treatment*, and *tests*, tag nothing. For *symptoms*, *treatment*, and *tests*, coverage is saturated (95–98%), so nearly every patient is covered and the gate allows almost everyone. For *history* (coverage 42.8%) and *observation* (coverage 1.3%), the gate simply does not fire on this cohort. The mechanism operates correctly but rarely activates.

Fallback (no NER bucket). *adverse_event* and *outcome_mortality* have no matching NER bucket, so the fifth source cannot apply and the difficulty gate runs, tagging PASS pairs only ($P(t | F) = 0$).

The net picture is an operating envelope rather than a uniform effect: strong per-patient selectivity in two categories, coarse categorical filtering in two, no measurable tagging in five, and no application in two. The gate is selective in the mid-to-high-coverage regime where the coverage signal separates the PASS and FAIL strata, and degenerates predictably outside it. Identifying these conditions is itself a methodological contribution.

Per-category instability for small FAIL strata. The per-category lifts for categories with small FAIL strata (*diagnosis*, $n_{\text{FAIL}} = 105$; the outcome categories, $n_{\text{FAIL}} \leq 451$; *adverse_event*, $n_{\text{FAIL}} = 447$) are subject to run-to-run noise. An independent replication under the full-DBPM configuration (the cross-task ablation arm, Appendix A.7) gave a path lift of 1.71, within the 1.52–1.84 band, but the per-category *diagnosis* lift swung between near-zero and large positive values across runs and configurations of the same gate. We caution against drawing per-category conclusions from any single run: the aggregate path lift is stable, the per-category lifts on small strata are not. The regime-level classification (selective, categorical, saturated, fallback) is robust across runs even where the precise within-regime lifts vary.

Table 9

Pair-count deltas between the full-DBPM ON and OFF arms on the held-out cohort. The named-entity (+0.19%) and QA (−0.03%) deltas are within the per-stage non-determinism floor, confirming that the NER-coverage gate tags QA candidates without removing them. The relation delta (−913, −0.74%) is the Ontology-Violation Filter’s genuine suppression, the only above-noise pair-count change.

Stage	ON	OFF	Δ	$\Delta\%$
NER	133,790	133,533	+257	+0.19%
RE	122,425	123,338	−913	−0.74%
QAR	31,135	31,143	−8	−0.03%

Table 10

Tagging summary on the held-out cohort (DBPM-full ablation) across all eleven QA categories. Rows are the verifier’s verdict; columns are the gate’s tag (DOWNGRADE collapsed with BLOCK as *tagged*). Percentages are within-row, the fraction of each verdict class that the gate tags, so each row sums to 100%. The table reports selectivity, not classification accuracy: the gate is a selective tagger on a single grounding signal, not a verifier surrogate, so the relevant quantity is the ratio of the two tag rates (the lift), not precision, recall, or F1. The gate tags 36.0% of verifier-FAIL pairs against 19.6% of verifier-PASS pairs, a lift of $0.360/0.196 = 1.84$ (95% CI [1.75, 1.93]). Tagging in the nine mapped categories is produced by the NER-coverage gate; the two no-bucket categories (*adverse_event*, *outcome_mortality*) are tagged by the difficulty gate, which contributes no FAIL-side tags, so the all-category ratio equals the mapped-category path lift, an equality specific to these data, not a general identity.

Verifier verdict	Tagged	Not tagged	Row total
FAIL	1,392 (36.0%)	2,476 (64.0%)	3,868
PASS	6,101 (19.6%)	25,034 (80.4%)	31,135
Column total	7,493	27,510	35,003

6.5. Tagging, Not Suppression: Measurement Discipline and Provenance

Under the DOWNGRADE-first discipline, the NER-coverage gate tags pairs without removing them, so the gate produces almost no change in pair counts even while tagging thousands of pairs. Table 9 shows the pair-count deltas and Figure 6 contrasts them against the tagging volume.

The gate tagged 6,101 verifier-PASS QA pairs in the ON arm against zero in the OFF arm (where the master switch deactivates every mechanism), so all 6,101 PASS-side tags are attributable to DBPM. With the 1,392 FAIL-side tags, 7,493 QA pairs are tagged in total, the basis of the confusion summary in Table 10. Against this tagging volume, the near-zero pair-count deltas confirm the design intent: selectivity must be read from tagging behaviour, not output volume.

Aggregate DBPM provenance (single combined ablation). A single paired ablation toggles all new DBPM mechanisms together via the master switch. On the same held-out cohort it produced 913 silent relation suppressions by the Ontology-Violation Filter (ON arm 122,425 relations against 123,338 in the OFF arm) and 6,101 attributable QA downgrade-tags by the NER-coverage gate (against zero when the switch is off). Together these are 7,014 gating events across the 287,350 pipeline pairs of the ON arm, or 2.44% of pipeline pairs touched by the new DBPM mechanisms.

The combined-ablation suppression count of 913 differs from the isolated count of 1,207 (Section 6.2) because the two ablations differ in *both* arms, not only the OFF arm: the isolated ablation holds the NER-coverage gate ON in both arms and measures only the Filter, whereas the combined ablation turns every mechanism off together, which shifts the relation pair counts in both arms as well. The two numbers are not in conflict; each is the right answer to a different question. The combined figure of 913 answers “What is DBPM’s aggregate contribution against an ungated baseline?”; the isolated figure of 1,207 answers “What is the Filter’s contribution holding everything else constant?”

At this scale, the allow-set dominates the blocklist: the named-entity channel holds 96,708 whitelisted signatures against 2,991 blocklist patterns, and the QA channel holds 11 whitelisted signatures against 34 blocklist patterns. This dominance is consistent with the early-ALLOW exit of Equation (4): most candidates match a known-safe signature and bypass belief-based gating.

Table 11

The five signal sources tested for the question-answering gate, characterised by what each read, its granularity, the empirical outcome, and the failure mode where applicable. The NER-coverage gate is the working design; its path lift band of 1.52–1.84 is measured across four independent replications (Section 8.3).

Source	Signal read	Granularity	Outcome	Failure mode
Category-aggregate fail-mass	category-aggregate verifier fail-mass	category-level	anti-selective (lift 0.006)	aggregation-level mismatch
Verifier uncertainty	verifier parse-failure flag	per-pair	signal absent	signal absence
Per-category fail-rate	per-category fail-rate (dual-bucket)	category-level	anti-selective (lift 0.05)	counting asymmetry
Per-patient difficulty	per-patient upstream difficulty	per-patient, cross-task	no signal (lift 0.00)	cross-task orthogonality
NER-coverage intersection	per-patient NER-category coverage	per-patient, cross-task	selective (path lift 1.52–1.84 across four replications)	working design

Runtime overhead. The ON arm ran in 8h48m10s (6.34 s/patient) and the OFF arm in 8h48m50s (6.35 s/patient), a difference of 40 seconds across 31,690, or 0.13%. This is below the pipeline’s per-patient variance floor (expected noise on the mean across $n = 5000$ is roughly ± 140 seconds; continuous batching, the dual-model verifier, and network jitter contribute 1–3 seconds of per-patient standard deviation). We therefore claim only that the gate’s per-patient overhead is below the variance floor, not that it produces a speed-up.

Two consequences follow for downstream consumers. First, DBPM’s gate is measurement-instrumented rather than production-suppressive: it records which pairs *would* be blocked under hard-BLOCK mode without committing to the removal, and a deployment wishing to act on its verdicts would enable hard-BLOCK mode (Section 4.9). Second, in Table 9 the named-entity and QA deltas are within non-determinism, and the relation delta of -913 is the Filter’s suppression, not a gate effect; the gate itself, in DOWNGRADE-first mode, removes no pairs. Conclusions from DBPM ablations must therefore be drawn at the tagging level, not from pair-count deltas.

Provenance scope. The 2.44% figure comes from a single master-switch ablation on the locked cohort, measuring the aggregate contribution of the two new mechanisms against an ungated baseline on identical input. Pattern-level cross-task propagation is disabled in both arms by the master switch; its independent contribution is measured separately in Appendix A.7 at 0.098% of pipeline throughput, below the per-stage non-determinism floor.

7. Discussion

This section sets out what the results of Section 6 establish about inference-time pattern-memory gating in LLM-grounded clinical NLP. We organise it around three questions: what the five-source dissection of the question-answering gate reveals as a structural principle (Section 7.1); how the production-scale failure of the verifier-fed channel changes the design problem for downstream pipelines (Section 7.2); and what follows for the safe deployment of LLM-driven extraction at scale (Section 7.3).

7.1. A Structural Principle for Selective Pre-Generation Gating

The five-signal dissection of the question-answering gate (Sections 4.8 and 6.3) is enough to state a structural principle about which signals can make inference-time gating selective in a generator-verifier architecture. In each of the first four gate variants, the gate read a structurally distinct signal and failed for a structurally distinct reason; the fifth succeeded by reading a signal none of the others did. Table 11 lays out the progression.

Read across the five, the pattern is *not* that more sophisticated mechanisms win. The second and fourth sources are more elaborate than the first, and they fail more conclusively. The pattern is that a pre-generation signal is selective for verifier rejection only when it directly probes the answer-grounding question the verifier itself evaluates. The first and third gate variants test a category-level statistic, the accumulated fail-mass or fail-rate of the whole category, but

the verifier accepts or rejects each pair individually, so a category-level signal cannot separate the pairs the verifier distinguishes within that category. The second variant checks a parse-failure flag, on the assumption that unparseable output marks an uncertain verdict, but modern instruction-tuned models almost always produce parseable output, so the flag is essentially never set and carries no information. The fourth variant checks how much upstream extraction the patient required, on the assumption that hard-to-extract patients yield worse answers; but the verifier judges the answer's own content, whether it is hallucinated, over-specified, or unsupported by the source text, and this is unrelated to upstream extraction difficulty. We confirmed the two are unrelated directly: the upstream-difficulty scores of verifier-passed and verifier-failed pairs are statistically indistinguishable (Section 6.3). The fifth variant checks whether the patient has the extracted clinical entities that an answer in the asked category would need, which is the same question the verifier resolves when it decides whether an answer is grounded. That alignment between the gate's signal and the verifier's decision criterion is what makes the fifth variant selective.

The principle is directly usable. A practitioner designing an inference-time gate for a generator-verifier pipeline can test a candidate signal by asking whether it probes the same question the verifier answers. If it does, the gate may be selective; if it does not, the gate will not be, however sophisticated its aggregation. The five sources give one positive and four negative instances of exactly this test.

Alignment is necessary for selectivity but does not guarantee it. The four failed variants establish the necessary half: none was selective, and none probed the verifier's grounding question. But alignment alone is not sufficient, a signal can probe the right question and still fail to separate PASS from FAIL when its values do not vary across patients. The per-category operating envelope (Section 6.4) shows this: even the well-aligned NER-coverage signal degenerates under coverage saturation, where nearly every patient has the relevant entities and the gate rarely fires, and under coverage sparsity, where nearly no patient has them and the gate fires categorically rather than per patient. Signal-distributional properties bound the operating regime beyond the alignment requirement.

The principle also explains an interaction between the Ontology-Violation Filter and the NER-coverage gate. In isolation, the `diagnosis` category is anti-selective, but under full DBPM it becomes the most selective category (lift 17.13, Section 6.4). The Filter removes ontology-violating relations that would otherwise enter the coverage signal the gate reads; with those spurious relations gone, the coverage signal aligns more closely with the verifier's grounding decision for diagnosis questions. This is the principle operating one level up: cleaning an upstream signal makes a downstream signal more aligned with the verifier's question, and so more selective.

7.2. Verifier-Fed Memory as a Production-Scale Failure Mode

The empty verifier-fed relation-extraction channel at production scale (Section 6.1), zero persisted patterns against 785,797 logged classifier rejections, is a production-scale failure of the most natural design for an inference-time pattern memory. That design accumulates per-signature rejection statistics through a source-weighted update (Equation 3), applies time-decay so the memory can recover as documentation conventions shift (Equation 5), and prunes signatures whose decayed severity falls below a floor. Each mechanism is individually sensible; their interaction at production scale is not.

What determines the outcome is the distributional shape of the rejection stream, not its volume. When rejections concentrate, many failures sharing a few signatures, each signature is reinforced faster than it decays and clears threshold. When rejections disperse, many failures spread thinly across many signatures, each signature decays between save events faster than reinforcement arrives, and nothing clears threshold no matter how high the total volume. Across the full 167,034-patient run, the relation rejection stream was dispersed: its 785,797 rejections spread across the open natural-language vocabulary of relation labels the model emits, with no single signature reinforced fast enough to survive.

The Ontology-Violation Filter (Section 4.7) avoids this failure by changing the source of the signal that feeds the channel, not the persistence mechanism. Its predicate fires per candidate against a fixed set of 29 type-triples, so events concentrate on those triples regardless of how the relation label is phrased. The concentrated distribution clears threshold where the dispersed one did not, and it does so through the same persistence machinery; only the input signal differs. The contribution here is the empirical demonstration that the choice of input signal, the verifier's verdicts versus the ontology predicate, not the design of the memory, can be the difference between an empty channel and a populated one across the full 167,034-patient run.

The implication reaches past this pipeline. Any inference-time memory that accumulates per-signature statistics over free-form LLM output, whether relation labels, classification tags, or intent labels, is exposed to the same

dispersion. The remedy is to define signal sources that map that free-form output onto a bounded canonical space, so the channel concentrates rather than disperses.

7.3. Clinical Implications

Three findings of this paper carry directly into clinical deployment practice: a pattern-memory blocklist can be configured yet empirically empty at scale, an ontology signal and a verifier catch different error classes and so complement rather than replace each other, and tagging suspect candidates rather than deleting them keeps every gating decision in the clinical audit trail. We state each as an implication for practitioners adopting inference-time pattern-memory gating in LLM-grounded extraction pipelines.

(i) *A blocklist that appears configured may be empirically inactive.* Section 6.1 documents a verifier-fed relation blocklist that was empty at production scale even though the pipeline generated nearly 800,000 rejections that should, in principle, have filled it. A pipeline that relied on this blocklist for a safety guarantee would have shipped without that guarantee being enforceable on its full corpus. The lesson is that a deployment using a pattern-memory gate needs observability for whether the memory *actually populates* at scale, not merely confirmation that the mechanism is configured to populate it. We release the `crosscheck_F1_167k_blocklist.py` script as one such check.

(ii) *Verifier-independent signal sources complement rather than replace the verifier.* The Ontology-Violation Filter fills the relation blocklist where the verifier-fed pathway did not, but the two are not redundant. The verifier rejects relations on content grounds (hallucinated pairs, unsupported relations); the Filter rejects them on structural grounds (type-triple violations against the ontology). On the held-out cohort, the Filter flagged 49,734 ontology violations while the verifier continued to reject content errors on a separate set of candidates. A deployment seeking coverage of both error classes should run both sources.

(iii) *Tagging rather than blocking preserves auditability.* Automated removal of model output is contentious in clinical settings, because a wrongly removed candidate is invisible by construction and therefore impossible to audit. The DOWNGRADE-first discipline (Section 4.9) tags suspect candidates in the output stream instead of removing them, so downstream consumers, clinicians, auditors, and training pipelines alike, see exactly what the gate flagged and decide for themselves whether to act. A hard-blocking configuration is available for deployments that prefer the gate's verdict to be final. We recommend the tagging default in clinical contexts because a flagged candidate stays in the audit trail whereas a blocked one disappears from it. This is an interpretive recommendation following from the measurement discipline; the present work does not directly compare the costs of a false block against those of a false allow in clinical use.

8. Limitations

The empirical claims face four principal threats to validity, which we address in turn: the narrow operating envelope of the NER-coverage gate (Section 8.1); the absence of a measured downstream precision lift (Section 8.2); construct overlap between the gate's design hypothesis test and its deployment evaluation (Section 8.3); and single-corpus evaluation on PMC-Patients (Appendix A.8, consolidated in Section 8.4). We disclose each so that readers and reviewers can locate the bounds of the claims.

8.1. Operating-Envelope Bounds of the NER-Coverage Gate

The NER-coverage gate is selective in one operating regime, mid-spectrum coverage, and degenerates in others. The per-category breakdown on the held-out cohort (Section 6.4) identifies four regimes.

- **Selective** (`diagnosis`, `risk_factor`): the gate separates PASS from FAIL pairs. `diagnosis` (lift 17.13 at 95.7% coverage) tags 73% of FAIL pairs against 4% of PASS pairs; `risk_factor` (lift 2.16 at 53.7% coverage) tags all FAIL pairs and 46% of PASS pairs. `diagnosis` is selective only under full DBPM, where the Ontology-Violation Filter cleans the upstream coverage signal (Section 7.1).
- **Categorical** (`outcome_clinicalstatus`, `outcome_disposition`): at sparse coverage (4.4% and 1.7%) the gate tags nearly uniformly (lift 1.05 and 1.02), behaving as a category-level filter rather than a per-patient gate.

- **Saturated or no-tagging** (history, observation, symptoms, treatment, tests): for symptoms, treatment, and tests, coverage above 95% means nearly every patient is covered and the gate allows almost everyone; for history and observation, the gate does not fire on this cohort. In both sub-regimes, the mechanism operates correctly but rarely activates.
- **No NER bucket** (adverse_event, outcome_mortality): the worker has no matching bucket, so the gate cannot apply and the difficulty-gate fallback tags PASS pairs only.

The headline path lift of 1.84 therefore averages behaviour across these regimes. A deployment seeking uniform selectivity across all eleven categories would need to address the saturated, sparse, and no-bucket regimes through schema closure (Section 9.1) and category-specific configuration.

8.2. No Downstream Precision Lift Measured

The verifier is permissive at the scale tested: it passes essentially every relation reaching the enriched output stage in both arms of both ablations. The precision proxy delta on the held-out cohort is therefore 1.0000/1.0000, and we cannot claim that DBPM reduces downstream hallucinations as measured by the verifier's decisions on enriched output.

What DBPM demonstrably does is upstream candidate suppression (the Ontology-Violation Filter removes 913 relation candidates on the held-out cohort) and per-pair selectivity tagging (the NER-coverage gate tags 6,101 PASS-side QA pairs against a fully ungated baseline; Section 6.5). These are measurable effects on the pipeline's intermediate state, not measured improvements to the final dataset's clinical correctness. Establishing that the algorithmic effects translate into clinical-correctness gains requires human-rated true-positive evaluation on a stratified sample of suppressed and tagged candidates, which is outside this paper's scope (Section 9.2) and reserved for separate dataset-quality work.

8.3. Construct Overlap in the Gate's Hypothesis Test

The development-cohort hypothesis test that motivated the NER-coverage gate used the same construct, per-patient NER coverage against per-patient QA failure, that the deployed gate now reads as its decision signal. The lift measured on that cohort is therefore not a held-out estimate of the gate's generalisation.

We partially mitigate this by triangulating the path lift across four measurements under different configurations and runs: the component-isolated ablation on the held-out cohort gives 1.52, the cross-task full-configuration ablation gives 1.71, the full-DBPM held-out ablation gives 1.84, and the development cohort gives a global blended lift of 1.59.² The three path-lift measurements span 1.52–1.84, and every figure exceeds the 1.5 selectivity threshold. The full-DBPM configuration, which we adopt as the primary result, sits at the top of this band because the Ontology-Violation Filter removes ontology-violating relations that would otherwise inflate the coverage signal, sharpening it when the full stack is active (the `diagnosis` category, for instance, rises from anti-selective in isolation to a lift of 17.1 under full DBPM; Section 6.3). Replication across scales, configurations, and runs is not the same as held-out generalisation, but the consistency of the path lift above threshold across every measurement strengthens the mitigation. A genuine held-out validation would require a fresh cohort drawn from a population the hypothesis test did not consume; we identify this as future work (Section 9.3).

8.4. Further Limitations in Appendix A.10

Two further limitations are retained in Appendix A.10 so the body stays focused on the three principal bounds above:

- Pattern-level cross-task propagation (Section 4.4), previously flagged as not independently ablated, is now measured at 0.098% of pipeline throughput, below the per-stage non-determinism floor (Appendix A.7).
- Single-corpus evaluation: all results are measured on PMC-Patients; extension to electronic health record (EHR) corpora is reserved for future work (Section 9.3), with the structural expectations under EHR distribution shift discussed in Appendix A.8.

²The development-cohort entry is the *global* blended lift (1.59), not the path lift (1.89 on the nine mapped categories, Section 6.3); we list it here because it is the figure the hypothesis test reported, and we mark it as global to avoid conflating it with the three path-lift measurements.

8.5. Scope of the Methodological Contribution

This paper makes claims about DBPM's algorithmic behaviour: which signal sources populate which channels, which gate designs are selective, and which integrity checks pass at scale. It does *not* claim that DBPM's outputs improve the clinical correctness of the resulting dataset, that the suppressed relations are genuinely wrong in the clinical context of their source text, or that models trained on DBPM-gated output outperform those trained on ungated output. These are downstream-quality questions for separate evaluation work, deferred explicitly to keep the present scope coherent.

9. Future Work

We identify three future-work directions, ordered by how directly they extend the paper's contributions. Each addresses a specific limitation from Section 8.

9.1. Schema Closure for No-Bucket Categories

Two categories (`adverse_event`, `outcome_mortality`) have no matching NER bucket, so the NER-coverage gate cannot fire and the difficulty-gate fallback tags PASS pairs only (Sections 6.4 and 8.1). Extending the NER stage to emit `Adverse_Event` and `Outcome_Mortality` entity types would let the gate operate on these two categories on the same terms as the other nine. Closing the schema this way would raise the *global* blended lift toward the path lift, since the two fallback categories would begin contributing selective tags rather than zero-lift fallback tags; the realised gain depends on the NER yield in these categories and the verifier's rejection distribution within them, and is an empirical question for the closed-schema deployment. Schema closure is an engineering extension that does not change the methodological contribution, but it is the most direct path to broadening the gate's operating envelope.

9.2. Dataset-Quality Evaluation

This paper makes no claim that DBPM's suppressions and tags improve dataset quality (Section 8.5). Establishing that would require a separate programme on the pipeline's multi-task derivative of PMC-Patients: stratified human review of suppressed relations and tagged QA pairs against clinical-correctness criteria, together with downstream model-training studies on gated versus ungated output. A stratified sample of suppressed relations across the six ontology-violation patterns has been prepared as a release artefact; its evaluation is reserved for a separate dataset-quality paper.

9.3. Held-Out and EHR Validation

The construct-overlap caveat (Section 8.3) is addressable by validating the gate on a held-out PMC-Patients cohort drawn from a population the hypothesis test did not consume. The single-corpus caveat (Appendix A.8) is addressable by extending evaluation to EHR-derived narratives, subject to the data-access constraints typical of EHR research. The two validations are complementary: the first establishes that the gate generalises on a similar distribution, the second that it generalises across a documentation-style shift. Each warrants its own publication.

10. Conclusion

DBPM is an inference-time pattern-memory gating mechanism for a clinical NLP pipeline, and this paper characterises its empirical behaviour at production scale rather than its theoretical properties. The characterisation yielded four findings: a verifier-fed accumulation pathway that fails at 167,034-patient production scale (Section 6.1); a verifier-independent ontology pathway that succeeds where the verifier-fed pathway did not (Section 6.2); a five-source dissection of the question-answering gate in which four sources fail for structurally distinct reasons and one succeeds by aligning its signal with the verifier's grounding criterion (Sections 6.3 and 6.4); and the structural principle that follows from the dissection (Section 7.1).

The gate's operating envelope is bounded. We characterise the bounds, saturated coverage, sparse coverage, categorical regimes, and no-bucket categories (Section 8.1), and identify the extensions that would expand them. We do not claim improvements to downstream clinical correctness: the effects we measure are upstream candidate suppression and per-pair selectivity tagging, and whether these translate into clinically correct dataset improvements is reserved for separate dataset-quality work (Section 9.2).

The five-source dissection is the contribution we expect to travel beyond this pipeline. Practitioners designing inference-time gates for generator-verifier architectures in any domain, clinical NLP, code generation, scientific

extraction, agentic tool use, can apply the structural principle to test a candidate signal source before investing engineering effort in a mechanism that the four negative results here suggest will not generalise. The principle is necessary, not sufficient: signal-distributional properties further bound the operating regime. Both the principle and the bounds emerge from work at production scale, where the failure modes the paper documents become visible in a way they do not at benchmark scale.

We release the DBPM gating module, the ablation runner, the gate-decision graders, and the held-out cohort identifier list. The release lets any reader reproduce the source-by-source outcomes and the production-scale channel finding from the same underlying data; the five signal sources are documented as a repository changelog.

A. Implementation, Operational, and Extension Details

This appendix collects implementation engineering, operational configuration, and extension-direction material referenced from the body of the paper. Section A.1 also serves as the in-code identifier reference for the mechanisms that Section 4 names by function: the body names each flag, threshold, and method by what it does, and the mapping to source-level identifiers is given here.

A.1. Implementation and In-Code Identifier Reference

DBPM is realised as a single Python class with $\mathcal{O}(1)$ amortised gate cost. Read-side data structures are precomputed once per save into per-task hash sets `_block`, `_downgrade`, `_whitelist`, indexed by signature; gate queries (Equation 4) are constant-time set membership with at most three lookups (whitelist, block, downgrade) plus a count comparison. Write-side updates (Equations 2 and 3) use a `_write_index` mapping signature keys to pattern dictionaries for $\mathcal{O}(1)$ in-place modification.

State is persisted to a single JSON file (`bpm_production.json`) under a FileLock-protected atomic-write protocol: the in-memory state is serialised to a temporary file and renamed over the canonical path under exclusive lock. To bound I/O contention at the deployment's 64-way effective concurrency, saves are batched: each worker process accumulates record events and triggers a save after every 200 such events, then merges the on-disk state with its own using max for severity and sum for counts. With 16 worker processes, this places save frequency at roughly one merge per 12.5 events globally, below the FileLock acquisition rate threshold for serialisation stalls.

Gate methods and signal sources. The three gate sites of the three-tier policy (Section 4.5) are exposed as `gate_ner(σ , NER)`, `gate_relation(σ , RE)`, and `gate_qa(category, ...)`. The question-answering method retains the legacy name `gate_qa` for backward compatibility; the deployed configuration runs on QAR-category inputs, and all selectivity claims are measured against QAR outputs (Section 3.1). The Ontology-Violation Filter (Section 4.7) is M3-RE in the codebase: it records through `bpm.record("re", payload, failure_type="hard_fail")` with payload field `onto_violation=True`, and populates the same `_re_block` cache that `gate_relation()` queries, introducing no new gate.

Ablation flags. Six flags expose the design choices for ablation (Table 12). The four core flags toggle individual mechanisms; the gate-level flag `M1_QA_GATE_HARD_BLOCK` controls whether the question-answering gate emits BLOCK at all and defaults to 0 (DOWNGRADE-first) in every measurement of this paper (Section 4.9); and the master switch `BPM_DISABLE` disables all DBPM gating and recording by flipping the four core flags to OFF at worker initialisation. Because the master switch operates at gate-invocation time rather than at configuration-serialisation time, the persisted configuration block is byte-identical between a `BPM_DISABLE=0` run and a `BPM_DISABLE=1` run; the architectural consequences of this are discussed in Section A.6.

Thresholds and constants. Table 13 maps the concept names used in Section 4.2 to their in-code identifiers and deployed values. The learning rates and decay factors are given in Table 3 and the body of Section 4.2; the source weights are in Table 4. The question-answering fail-rate threshold of the third and fourth signal sources (Equations 7 and 8) is `M1V5_FAIL_THRESHOLD`, set to 0.30 on the development cohort and 0.60 on the held-out 5,000-patient cohort; the difficulty threshold of the fourth source is `M1V6_DIFFICULTY_THRESHOLD = 0.30`.

Memory state and persistence fields Each blocklist entry stores the tuple $(\sigma_{\text{sev}}, c, \tau_{\text{last}}, \kappa)$ of Section 4.3 under `tasks[t].patterns` in `bpm_production.json`, with the cross-task hit counter κ held in the field `cross_task_hits`; whitelist entries are stored under `whitelist[t]` as $(\sigma_{\text{conf}}, c, \tau_{\text{last}})$. Rejection events are logged to

Table 12

Module-level ablation flags and their effect. The default column gives the value used in the deployed full-DBPM configuration; the master switch BPM_DISABLE overrides the four core flags when set.

Flag	Effect when OFF	Default
BPM_ENABLE_CROSS_TASK	No pattern-level cross-task propagation	ON
BPM_ENABLE_THREE_TIER	Gate collapses to BLOCK / ALLOW	ON
BPM_ENABLE_UNCERTAINTY	Ambiguous QAR verdicts treated as success	ON
BPM_ENABLE_SOURCE_WEIGHTS	All source weights set to $w_s = 1$	ON
M1_QA_GATE_HARD_BLOCK	QAR gate emits DOWNGRADE, never BLOCK	0
BPM_DISABLE	All DBPM gating and recording active	0

Table 13

Concept-to-identifier mapping for the thresholds and constants of Section 4.2. Per-task values are given as (NER, RE, QAR).

Concept (body)	In-code identifier	Deployed value
Block threshold θ_i^{block}	BLOCK_THRESHOLDS[t].min_severity	(0.65, 0.70, 0.60)
Minimum support n_i^{min} (block)	BLOCK_THRESHOLDS[t].min_count	(3, 2, 3)
Downgrade threshold θ_i^{down}	downgrade band lower bound	0.40 (all tasks)
Minimum support (downgrade)	–	1 (all tasks)
Storage cap C_i	per-task pattern cap	(200, 300, 150)
Severity-zone guard	cross-task severity ceiling	0.55
Propagation cap	cross_task_hits ceiling	3
QAR fail-rate threshold	M1V5_FAIL_THRESHOLD	0.30 dev / 0.60 held-out
QAR difficulty threshold	M1V6_DIFFICULTY_THRESHOLD	0.30
DOWNGRADE confidence multiplier	calibrated-confidence scale	0.70

universal_rejections.jsonl as the tuple (uid, stage, entity, reason, conf) of Section 3.2. The deterministic question-to-category map consulted by the NER-coverage gate is QA_TEMPLATES_GEN; the ontology and alias tables of Equation (6) are ENTITY_RELATION_PRIORS (29 admissible type-triples) and RELATION_ALIAS (32 normalisation entries), both fixed at worker load time. The per-pair gate verdict is written to the output field dbpm_gate, the cross-task recursion guard of Algorithm 1 is the parameter is_cross_task, and the inactive self-critique source of Table 4 is gated by SELFVERIF_ENABLE, which defaults to OFF.

A.2. Verifier Verdict Semantics

A design choice of the surrounding pipeline is worth noting because it shapes the verdict distribution DBPM consumes. The verifier is conservative-pass on binary tasks: for NER, only an explicit “NO” yields FAIL, and ambiguous outputs default to PASS. For RE, ambiguous outputs default to PASS_WEAK, the middle of the graded scale. For QAR, a single ambiguous output triggers a three-vote ensemble with tie-break to PASS.

These conservative defaults reduce false-rejection on borderline candidates and produce a verdict distribution skewed toward acceptance, which is the appropriate prior in clinical extraction where over-rejection systematically loses recall on rare entities. DBPM’s gating policy (Equation 4) compensates by requiring n_i^{min} corroborating failures before a BLOCK fires, so the conservative-pass verifier and the support-count threshold work together rather than at cross-purposes.

Table 14

Complete experimental configuration. All settings were fixed before analysis and are reported here so the measurement and downstream experiments can be reproduced exactly. The gating constants summarised below are stated in full, with their in-code identifiers, in Tables 12 and 13; learning rates and source weights are in Tables 3 and 4.

Component	Setting
Pipeline and corpus	
Source corpus	PMC-Patients (167,034 patient narratives)
Generator model	Llama-3.3-70B (instruction-tuned)
Verifier model	MMed-Llama-3.1-70B
Task buckets	11 total; 3 DBPM-gated (NER, RE, QAR)
Serving framework	vLLM, continuous batching, tensor parallelism TP = 2 per model
Decoding (generator and verifier)	
Context window	8192 tokens (<code>-max-model-len</code>)
Max concurrent sequences	256 (<code>-max-num-seqs</code>)
GPU memory utilisation	0.90 (<code>-gpu-memory-utilization</code>)
Precision	<code>bfloat16</code> (<code>-dtype bfloat16</code>); chunked prefill enabled
Sampling temperature	0.0 (greedy) for all gated-task generation and verification
Top- p / top- k	Not applicable at temperature 0 (top- p 0.9 engaged only if temperature > 0); no top- k
Max generation tokens	Per stage: 1500 (RE/JSON extraction), 160 (QAR), 60 (verifier verdict)
DBPM gating	
Block thresholds θ_i^{block}	0.65 / 0.70 / 0.60 (NER / RE / QAR)
Downgrade threshold θ_i^{down}	0.40 (all tasks)
Minimum support n_i^{min} (block)	3 / 2 / 3 (NER / RE / QAR); 1 for downgrade
Storage caps C_i	200 / 300 / 150 (NER / RE / QAR)
Wall-clock half-lives h_i	5 / 10 / 10 days (NER / RE / QAR)
In-run decay ρ_v	0.99 (hard_fail), 0.985 (soft_downgrade)
Severity-zone guard	0.55 (cross-task severity ceiling)
Propagation cap	3 cross-task hits per signature
DOWNGRADE confidence multiplier	0.70
QAR fail-rate threshold	0.30 (development) / 0.60 (held-out)
QAR difficulty threshold	0.30
Measurement mode	DOWNGRADE-first (M1_QA_GATE_HARD_BLOCK = 0)
Evaluation cohort	
Held-out cohort	5,000 patients, stratified random subsample
Stratification	Age bucket \times gender \times document-length tertile (24 non-empty strata)
Tertile cut points	T1 \leq 1,931 < T2 \leq 3,121 < T3 characters
Sampling	Floor allocation then proportional residual; uniform random without replacement
Seed	Fixed (<code>random.Random(42)</code>)
Production cross-check	Full corpus, 167,034 patients, deployed DBPM-full configuration
Ablation protocol	
Paired ablations	3 (Ontology Filter; NER-coverage gate; full DBPM master switch)
Cross-task ablation	1 separate paired ablation (reported in Appendix A.7)
Selectivity metric	Lift = $P(\text{tag} \text{FAIL}) / P(\text{tag} \text{PASS})$
Significance	Delta-method 95% CI on log lift; H_0 : lift = 1
Hardware	
GPU	4 \times NVIDIA H200 (141 GB HBM3e each)
System	64 CPU cores, 900 GB system memory
Scheduler	SLURM (Supercomputing Wales Falcon)
Persistence	Single JSON file, FileLock atomic writes, 200-event save batches

A.3. Hardware and Software Configuration

Table 14 consolidates every fixed setting of the measurement, the models and their decoding parameters, the gating constants, the evaluation cohort, the ablation protocol, and the hardware, in a single reference; the remainder of this subsection expands the serving and concurrency configuration in detail.

Experiments run on a single SLURM-managed compute node: 4 \times NVIDIA H200 GPUs (141 GB HBM3e each), 64 CPU cores, 900 GB system memory. SLURM allocations are 72-hour wall-clock with a 70-hour Python-side budget and a 2-hour grace window for graceful shutdown.

The pipeline is deployed as two independent vLLM OpenAI-compatible API servers, the generator on port 8000 and the verifier on port 8001, each occupying two GPUs under tensor parallelism $TP = 2$:

- **Generator G .** Llama-3.3 70B (instruction-tuned) on GPUs 0–1, configured with `-max-model-len 8192`, `-max-num-seqs 256`, `-gpu-memory-utilization 0.90`, `-dtype bfloat16`, and `-enable-chunked-prefill`.
- **Verifier V .** MMed-Llama-3.1 70B (Qiu et al., 2024) on GPUs 2–3, with identical vLLM parameters.

The orchestrator spawns 16 worker processes via Python multiprocessing. Each worker maintains four concurrent patient coroutines, giving 64-way effective concurrency that vLLM’s continuous batching aggregates into efficient GPU batches. HTTP traffic between worker coroutines and the two vLLM servers is asynchronous (`aiohhttp`), with per-call timeouts of 180 s and three retry attempts. Running independent generator and verifier servers, rather than tensor-parallelising a single model across all four GPUs, avoids the larger cross-GPU synchronisation that a four-way split would incur. When one model is split across GPUs, the partial results each GPU computes must be summed and redistributed to every GPU before computation continues, an *AllReduce* collective operation that fires on every token; keeping each model within its own pair of GPUs confines this synchronisation to two GPUs rather than four. This is the configuration used for the production runs. The save-batching and FileLock protocol that bounds persistence contention at this concurrency is described in Section A.1.

A.4. Checkpoint-and-Resume Protocol

Because the full 167,034-patient corpus exceeds a single SLURM allocation, the pipeline implements a checkpoint-and-resume protocol. The orchestrator detects pre-existing `multitask_data_enriched.jsonl` output and skips already-processed UIDs, opening output files in append mode so no record is overwritten. The SLURM script monitors Python’s exit code and treats codes 124 (timeout fired with SIGTERM), 130 (SIGINT-handled), 137 (SIGKILL escalation), and 143 (clean SIGTERM exit) as resubmit-eligible, computing the remaining patient count and rebatching the job automatically.

DBPM state survives across job submissions because its JSON file is written to the shared output directory (`OUTPUT_DIR/bpm_production.json`), not to `node-local /tmp`.

A.5. Reproducibility

The DBPM gating module and the analysis artefacts required to reproduce the paper’s quantitative claims are released under an open-source license (see Code availability). The release includes:

- the standalone DBPM gating module (`dbpm.py`), with all numeric constants stated in Section 4.2 as class attributes;
- the selectivity grader (`grade_m1v7_selectivity.py`), the aggregate-provenance script (`aggregate_dbpm_provenance.py`), and the 167K cross-check (`crosscheck_F1_167k_blocklist.py`);
- the genericised ablation runner (`run_ablation.sh`), which documents the full-ON vs full-OFF protocol; and
- the held-out 5,000-patient and development-cohort identifier lists.

The surrounding extraction pipeline (the worker, orchestration, and model-serving layers) is not included; the released module is the gating logic the paper characterises, and the cohort lists plus aggregate counts permit reproduction of the reported selectivity, lift, and production-scale channel findings. The five question-answering signal sources are documented as a changelog in the repository rather than shipped as patch scripts against the withheld worker.

A.6. Architectural Disclosures

DBPM gates three of the eleven pipeline task buckets (NER, RE, QAR; Section 3.1). The summary task has a reserved threshold in `BLOCK_THRESHOLDS["summary"]` but no consumer gate. Medication extraction, temporal-event extraction, active-risk identification, risk-state-machine derivation, risk-based recommendations, risk-grounded QAR, and visualisation-payload assembly are entirely outside the DBPM gating system. Extension to these tasks is reserved for future work.

DOWNGRADE-first measurement discipline (Section 4.9) is applied to new, untested signal channels: the third signal source onward of the question-answering gate, and the Ontology-Violation Filter channel. Legacy production-validated channels (the named-entity gate over `_ner_block`, and the legacy `_re_block` check in `gate_relation`) retain hard-BLOCK semantics as a deliberate design choice, since they have empirical support from the project’s deployment history.

The byte-identical configuration footprint of the `BPM_DISABLE` master switch, noted in Section A.1, has one useful empirical consequence: because the switch acts at gate-invocation time, the OFF arm of the combined ablation (Section 6.5) records zero DOWNGRADE tags across the full 5,000-patient cohort, confirming that the switch produces the expected gate inactivity rather than a silently altered configuration.

A.7. Pattern-Level Cross-Task Propagation: Measured Contribution

The pattern-level cross-task propagation mechanism described in Section 4.4 is a persistence-layer component active in all DBPM runs reported in Section 6. We isolate its independent contribution via a single paired ablation: ON arm `BPM_ENABLE_CROSS_TASK = 1` (the deployed default) versus OFF arm `BPM_ENABLE_CROSS_TASK = 0`, with all other DBPM mechanisms (Ontology-Violation Filter, NER-coverage gate, three-tier gating, source weights) held at their default ON settings. Both arms use the held-out 5,000-patient cohort.

Result. The cross-task ablation produces a combined pair-count delta of 280 across the three gated tasks (NER $\Delta = -232$, RE $\Delta = +41$, QAR $\Delta = -7$) against 287,350 total pipeline pairs in the ON arm, yielding a contribution of 0.098% of pipeline throughput. This is below the 0.5% per-stage non-determinism floor of the pipeline (vLLM continuous batching plus the dual-model verifier introduce ~ 0.1 – 0.3% per-stage run-to-run variance on identical-cohort runs; see Appendix A.4). The path lift in the ON arm is 1.71, within the 1.52–1.84 empirical band documented in Section 8.3.

Instrumentation note. The worker’s `_event_counters["cross_task_propagations"]` global counter reported zero events in this ablation, while 24 NER patterns in the persisted `bpm_production.json` recorded `cross_task_hits > 0`. The discrepancy reflects an instrumentation gap in the worker’s event-counter update paths: cross-task propagation through new-signature creation increments the per-pattern counter but not the global event counter. The per-pattern evidence confirms the mechanism fired, and the pair-count delta is the authoritative measurement of mechanism contribution at the pipeline-output level. We disclose this for transparency; the substantive claim is the 0.098% pair-delta, which is independent of the global event-counter discrepancy.

Interpretation. The mechanism’s safeguards (severity-zone guard at 0.55, propagation cap $\kappa \geq 3$, source weights $w \in [0.2, 0.4]$) bound its impact below the per-stage non-determinism floor at the held-out 5K scale. This is consistent with the architectural intent of the mechanism: pattern-level cross-task propagation is designed to push severity into the DOWNGRADE band without crossing into BLOCK on cross-task evidence alone (Section 4.5, invariant 3), and at this scale the safeguards bind before any output-level effect accumulates. The result closes the independent-ablation limitation flagged in earlier drafts of this paper.

A.8. Single-Corpus Evaluation

All evaluation in this paper uses PMC-Patients (Zhao et al., 2023) as the source corpus. PMC-Patients is the established public benchmark for clinical narrative extraction at the sub-100K-patient-record scale, and using it permits direct comparison to prior LLM-driven clinical NLP work. However, the corpus consists of case reports from PubMed Central full-text articles, which differ in documentation style from electronic health records (EHRs) used in real clinical settings: case reports are authored for academic publication, are typically reviewed by peers before release, and are written with denotative precision intended to support reproducibility. EHR narratives are authored under clinical time pressure, contain abbreviations and shorthand specific to local institutional cultures, and reflect dictation artefacts not present in published case reports.

The empirical findings of Section 6, specifically the diffuse-rejection distributional shape that produced the production-scale channel finding (Section 6.1) and the per-category operating envelope of the NER-coverage gate (Section 6.4), may shift on EHR-derived corpora. Extension to EHR data is identified as future work (Section 9.3).

A.9. Answerability Cascade for Saturated and Sparse-Coverage Categories

Five QAR categories on the held-out cohort exhibit saturated NER coverage (symptoms, treatment, tests, observation, history); the NER-coverage gate rarely fires for these because nearly every patient is covered. One category (outcome_clinicalstatus) exhibits sparse NER coverage, so the gate fires categorically rather than per-patient. A complementary signal source, for example a distilled small-language-model answerability check that fires when NER coverage is uninformative, could extend the working operating envelope to these categories while preserving the deterministic predicate structure of the present design.

This extension is conditional on its own evaluation establishing that the additional signal is selective; we do not commit to it working at this stage. We identify it as the most natural next-step extension for deployments seeking uniform per-pair selectivity across all categories.

A.10. Limitations Addressed in This Appendix

This section consolidates the appendix-resident limitation disclosures referenced from Section 8.4:

- Pattern-level cross-task propagation (Appendix A.7): measured contribution 0.098% of pipeline throughput, below the per-stage non-determinism floor.
- Single-corpus evaluation (Appendix A.8): all empirical findings are measured on PMC-Patients; EHR distribution-shift is addressed in Section 9.3.

CRedit authorship contribution statement

Ali H. Lazem: Conceptualization, Methodology, Software, Validation, Formal analysis, Investigation, Data curation, Writing – original draft, Writing – review & editing, Visualization. **William Teahan:** Conceptualization, Methodology, Supervision, Writing – review & editing, Project administration.

Code availability

The DBPM gating module, the grader scripts that reproduce the reported selectivity and lift figures, and the cohort identifier lists are openly available on GitHub at <https://github.com/Ali-Lazem/DBPM> and permanently archived on Zenodo at <https://doi.org/10.5281/zenodo.21038023>. The surrounding extraction pipeline is not included; the repository provides the gating logic and the artefacts required to reproduce the paper’s quantitative claims.

Data availability

The cohort identifier lists used for the reported ablations are included in the code repository and index the publicly available PMC-Patients corpus (Zhao et al., 2023). The aggregate gating-outcome counts that reproduce the reported figures are provided in the repository (counts and rates only; no clinical text). The derived extraction corpus is not released.

Acknowledgements

We acknowledge the services of Supercomputing Wales and the Bangor eResearch Team, including the support provided by Dr. Ade Fewings.

References

- Alsentzer, E., Murphy, J., Boag, W., Weng, W.H., Jindi, D., Naumann, T., McDermott, M., 2019. Publicly available clinical bert embeddings, in: Proceedings of the 2nd Clinical Natural Language Processing Workshop, pp. 72–78.
- Aronson, A.R., 2001. Effective mapping of biomedical text to the umls metathesaurus: The metamap program, in: Proceedings of the AMIA Symposium, pp. 17–21.
- Borgeaud, S., Mensch, A., Hoffmann, J., Cai, T., Rutherford, E., Millican, K., van den Driessche, G., Lespiau, J.B., Damoc, B., Clark, A., et al., 2022. Improving language models by retrieving from trillions of tokens, in: International Conference on Machine Learning, pp. 2206–2240.
- Brown, T.B., Mann, B., Ryder, N., Subbiah, M., Kaplan, J., Dhariwal, P., Neelakantan, A., et al., 2020. Language models are few-shot learners, in: Advances in Neural Information Processing Systems, pp. 1877–1901.
- Chiang, W.L., Li, Z., Lin, Z., Sheng, Y., Wu, Z., Zhang, H., Zheng, L., Zhuang, S., Zhuang, Y., Gonzalez, J.E., Stoica, I., Xing, E.P., 2023. Vicuna: An open-source chatbot impressing gpt-4 with 90%* chatgpt quality. URL: <https://vicuna.lmsys.org>.

- Graves, A., Wayne, G., Reynolds, M., Harley, T., Danihelka, I., Grabska-Barwińska, A., Colmenarejo, S.G., Grefenstette, E., Ramalho, T., Agapiou, J., et al., 2016. Hybrid computing using a neural network with dynamic external memory. *Nature* 538, 471–476.
- Gu, Y., Tinn, R., Cheng, H., Lucas, M., Usuyama, N., Liu, X., Naumann, T., Gao, J., Poon, H., 2021. Domain-specific language model pretraining for biomedical natural language processing. *ACM Transactions on Computing for Healthcare* 3, 1–23.
- Henry, S., Buchan, K., Filannino, M., Stubbs, A., Uzuner, O., 2020. 2018 n2c2 shared task on adverse drug events and medication extraction in electronic health records. *Journal of the American Medical Informatics Association* 27, 3–12. doi:10.1093/jamia/ocz166.
- Hinton, G., Vinyals, O., Dean, J., 2015. Distilling the knowledge in a neural network. arXiv preprint arXiv:1503.02531.
- Hong, S., Zhuge, M., Chen, J., Zheng, X., Cheng, Y., Wang, J., Zhang, C., Wang, Z., Yau, S.K.S., Lin, Z., et al., 2024. Metagpt: Meta programming for a multi-agent collaborative framework, in: *International Conference on Learning Representations*.
- Kirkpatrick, J., Pascanu, R., Rabinowitz, N., Veness, J., Desjardins, G., Rusu, A.A., Milan, K., Quan, J., Ramalho, T., Grabska-Barwinska, A., Hassabis, D., Clopath, C., Kumaran, D., Hadsell, R., 2017. Overcoming catastrophic forgetting in neural networks. *Proceedings of the National Academy of Sciences* 114, 3521–3526. doi:10.1073/pnas.1611835114.
- Lee, D.H., 2013. Pseudo-label: The simple and efficient semi-supervised learning method for deep neural networks, in: *Workshop on Challenges in Representation Learning, ICML*, p. 896.
- Lee, J., Yoon, W., Kim, S., Kim, D., Kim, S., So, C.H., Kang, J., 2020. Biobert: A pre-trained biomedical language representation model for biomedical text mining. *Bioinformatics* 36, 1234–1240.
- Lewis, P., Perez, E., Piktus, A., Petroni, F., Karpukhin, V., Goyal, N., Küttler, H., Lewis, M., Yih, W.t., Rocktäschel, T., Riedel, S., Kiela, D., 2020. Retrieval-augmented generation for knowledge-intensive nlp tasks, in: *Advances in Neural Information Processing Systems*, pp. 9459–9474.
- Liang, J., Hu, D., Feng, J., 2020. Do we really need to access the source data? source hypothesis transfer for unsupervised domain adaptation, in: *International Conference on Machine Learning*, pp. 6028–6039.
- Lopez-Paz, D., Ranzato, M., 2017. Gradient episodic memory for continual learning, in: *Advances in Neural Information Processing Systems*.
- Madaan, A., Tandon, N., Gupta, P., Hallinan, S., Gao, L., Wiegrefe, S., Alon, U., Dziri, N., Prabhumoye, S., Yang, Y., Gupta, S., Majumder, B.P., Hermann, K., Welleck, S., Yazdanbakhsh, A., Clark, P., 2023. Self-refine: Iterative refinement with self-feedback, in: *Advances in Neural Information Processing Systems*. URL: <https://arxiv.org/abs/2303.17651>.
- Parisi, G.I., Kemker, R., Part, J.L., Kanan, C., Wermter, S., 2019. Continual lifelong learning with neural networks: A review. *Neural Networks* 113, 54–71.
- Park, J.S., O’Brien, J.C., Cai, C.J., Morris, M.R., Liang, P., Bernstein, M.S., 2023. Generative agents: Interactive simulacra of human behavior, in: *Proceedings of the 36th Annual ACM Symposium on User Interface Software and Technology (UIST)*, pp. 1–22.
- Qiu, P., Wu, C., Zhang, X., Lin, W., Wang, H., Zhang, Y., Wang, Y., Xie, W., 2024. Towards building multilingual language model for medicine. *Nature Communications* 15, 8384.
- Ratner, A., Hancock, B., Dunnmon, J., Sala, F., Pandey, S., Ré, C., 2019. Training complex models with multi-task weak supervision, in: *Proceedings of the AAAI Conference on Artificial Intelligence*, pp. 4763–4771.
- Santoro, A., Bartunov, S., Botvinick, M., Wierstra, D., Lillicrap, T., 2016. Meta-learning with memory-augmented neural networks, in: *International Conference on Machine Learning*, pp. 1842–1850.
- Savova, G.K., Masanz, J.J., Ogren, P.V., Zheng, J., Sohn, S., Kipper-Schuler, K.C., Chute, C.G., 2010. Mayo clinical text analysis and knowledge extraction system (ctakes): Architecture, component evaluation and applications. *Journal of the American Medical Informatics Association* 17, 507–513.
- Shinn, N., Cassano, F., Berman, E., Gopinath, A., Narasimhan, K., Yao, S., 2023. Reflexion: Language agents with verbal reinforcement learning, in: *Advances in Neural Information Processing Systems*. URL: <https://arxiv.org/abs/2303.11366>.
- Sukhbaatar, S., Szlam, A., Weston, J., Fergus, R., 2015. End-to-end memory networks, in: *Advances in Neural Information Processing Systems*.
- Tambe, M., 1997. Towards flexible teamwork. *Journal of Artificial Intelligence Research* 7, 83–124. doi:10.1613/jair.433.
- Taori, R., Gulrajani, I., Zhang, T., Dubois, Y., Li, X., Guestrin, C., Liang, P., Hashimoto, T.B., 2023. Stanford alpaca: An instruction-following llama model. GitHub repository. URL: https://github.com/tatsu-lab/stanford_alpaca.
- Teahan, W.J., Tuff, P.G., 2006. A framework for knowledge sharing between autonomous agents, in: *Proceedings of the 5th WSEAS International Conference on System Science and Simulation in Engineering*, pp. 219–227.
- Wang, D., Shelhamer, E., Liu, S., Olshausen, B., Darrell, T., 2021. Tent: Fully test-time adaptation by entropy minimization, in: *International Conference on Learning Representations*. URL: <https://openreview.net/forum?id=uX13bZLkr3c>.
- Wang, X., Wei, J., Schuurmans, D., Le, Q., Chi, E., Narang, S., Chowdhery, A., Zhou, D., 2023. Self-consistency improves chain-of-thought reasoning in language models, in: *International Conference on Learning Representations*.
- Wei, J., Wang, X., Schuurmans, D., Bosma, M., Ichter, B., Xia, F., Chi, E.H., Le, Q.V., Zhou, D., 2022. Chain-of-thought prompting elicits reasoning in large language models, in: *Advances in Neural Information Processing Systems*, pp. 24824–24837.
- Wettig, A., Gupta, A., Malik, S., Chen, D., 2024. Qurating: Selecting high-quality data for training language models, in: *Proceedings of the 41st International Conference on Machine Learning*, pp. 52915–52971.
- Wu, Q., Bansal, G., Zhang, J., Wu, Y., Li, B., Zhu, E., Jiang, L., Zhang, X., Zhang, S., Liu, J., et al., 2024. Autogen: Enabling next-gen llm applications via multi-agent conversation, in: *First Conference on Language Modeling*.
- Xie, Q., Luong, M.T., Hovy, E., Le, Q.V., 2020. Self-training with noisy student improves imagenet classification, in: *Proceedings of the IEEE/CVF Conference on Computer Vision and Pattern Recognition*, pp. 10687–10698.
- Yao, S., Zhao, J., Yu, D., Du, N., Shafraan, I., Narasimhan, K., Cao, Y., 2023. React: Synergizing reasoning and acting in language models, in: *International Conference on Learning Representations*. URL: <https://arxiv.org/abs/2210.03629>.
- Zhang, Q., Hu, C., Upasani, S., Ma, B., Hong, F., Kamanuru, V., Rainton, J., Wu, C., Ji, M., Li, H., Thakker, U., Zou, J., Olukotun, K., 2026. Agentic context engineering: Evolving contexts for self-improving language models, in: *International Conference on Learning Representations*. URL: <https://arxiv.org/abs/2510.04618>.

- Zhao, Z., Jin, Q., Chen, F., Peng, T., Yu, S., 2023. A large-scale dataset of patient summaries for retrieval-based clinical decision support systems. *Scientific data* 10, 909.
- Zheng, L., Chiang, W.L., Sheng, Y., Zhuang, S., Wu, Z., Zhuang, Y., Lin, Z., Li, Z., Li, D., Xing, E., Zhang, H., Gonzalez, J.E., Stoica, I., 2023. Judging llm-as-a-judge with mt-bench and chatbot arena, in: *Advances in Neural Information Processing Systems*.
- Zhou, C., Liu, P., Xu, P., Iyer, S., Sun, J., Mao, Y., Ma, X., et al., 2023. Lima: Less is more for alignment, in: *Advances in Neural Information Processing Systems*.

Ali Hussein Lazem received the B.Sc. in Computer Science from the University of Thi-Qar, Iraq, and the M.Sc. in Artificial Intelligence from Troy University, Alabama, USA. He is currently a Ph.D. candidate in the School of Computer Science and Engineering at Bangor University, United Kingdom. His research focuses on the production-scale deployment of large language models for clinical natural language processing, with broader interests in generative AI, computer vision, and machine learning.

William J. Teahan is a Senior Lecturer and Postgraduate Research Director in the School of Computer Science and Engineering at Bangor University, United Kingdom. His research spans natural language processing, text compression, machine learning, and agent-based systems, with a long-standing interest in statistical models of language and structured knowledge representation. He has contributed to multidisciplinary projects across computer science, biological sciences, and environmental sciences, with collaborations spanning multiple countries. His roles at Bangor include postgraduate supervision, curriculum development, and the coordination of research programmes within the School. He has supervised numerous doctoral students whose work has informed computational approaches to language modelling and applied artificial intelligence.

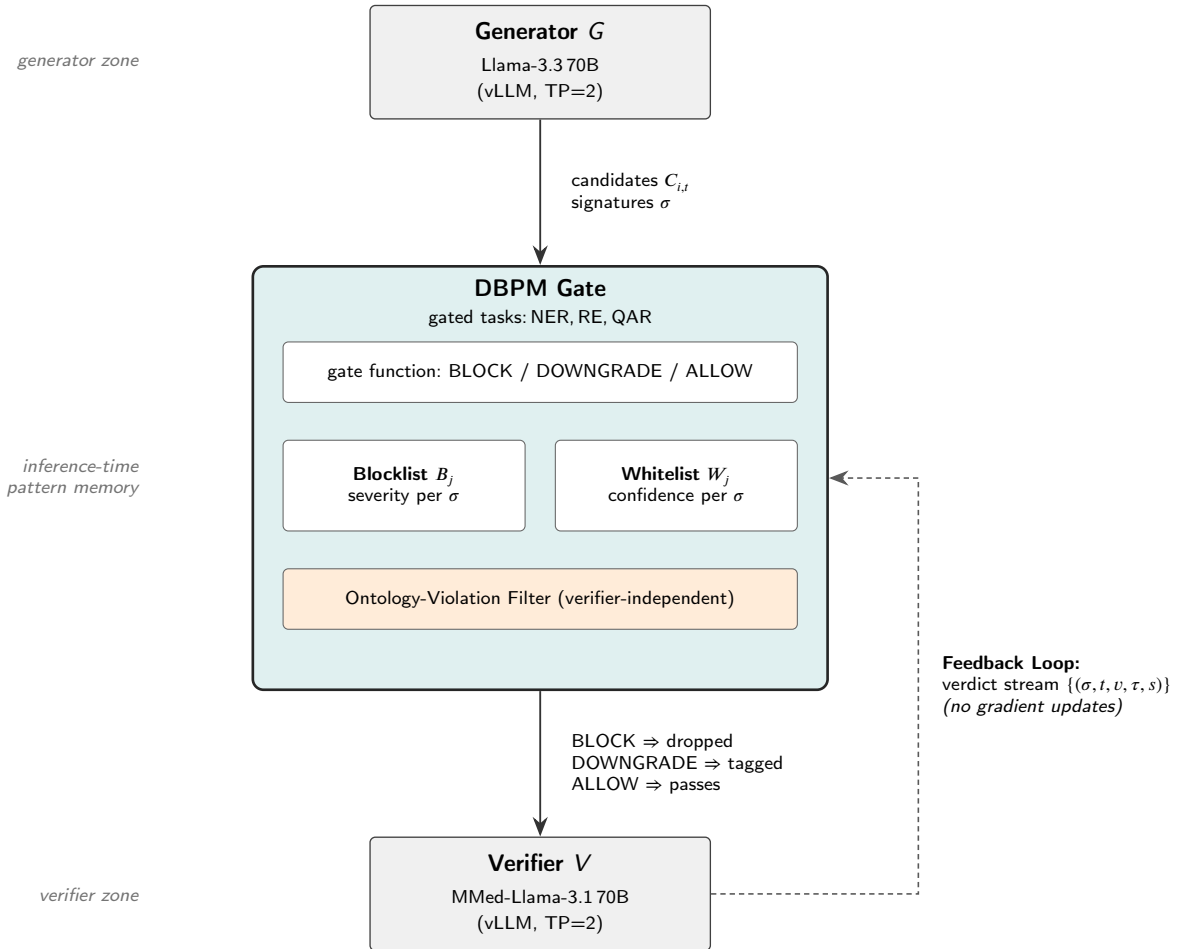


Figure 1: Architecture and locus of DBPM. The pattern memory sits between the generator (G , Llama-3.3 70B) and the verifier (V , MMed-Llama-3.1 70B). It gates candidate outputs before V is called (forward path, solid arrows) and accumulates evidence from V 's verdicts after each call (feedback loop, dashed arrow). The gate returns BLOCK, DOWNGRADE, or ALLOW for each candidate signature σ (Equation 4): a BLOCK'ed candidate is dropped before V is called, a DOWNGRADE'ed candidate passes through with a tag in its output metadata, and an ALLOW'ed candidate is unchanged. The dual store is the heart of the persistence layer (Section 4.3): the blocklist B_j accumulates severity evidence, while the whitelist W_j records direct verifier confirmation and takes precedence over indirect evidence. The Ontology-Violation Filter (Section 4.7) provides a verifier-independent signal source feeding the same blocklist. DBPM updates no parameters of G or V .

Algorithm 1 DBPM update operator U (per verdict event)

Require: verdict event (σ, t, v, τ, s) ; memory state (B_{j-1}, W_{j-1}) ; recursion guard is_cross_task (default FALSE)

Ensure: updated memory state (B_j, W_j)

- 1: **if** $v = \text{SUCCESS}$ **then**
- 2: update $W_{j-1}(\sigma, t)$ via the whitelist path ▷ whitelist path, Sec. 4.3
- 3: **return** (B_{j-1}, W_j)
- 4: **end if**

- 5: $\eta \leftarrow \eta_{v,t}; \quad w \leftarrow w_s$ ▷ learning rate, source weight
- 6: **if** entry e for (σ, t) exists in B_{j-1} **then**
- 7: $e.sev \leftarrow \min(1, \rho_v e.sev + w\eta)$ ▷ severity update, Sec. 4.3
- 8: $e.count \leftarrow e.count + 1; \quad e.\tau \leftarrow \tau$
- 9: **else**
- 10: initialise e with $sev = w\sigma_0(v)$, $count = 1$, $\kappa = 0$, $\tau = \tau$
- 11: insert e into B_j
- 12: **end if**

- 13: **if** is_cross_task **or** $v \neq \text{HARD_FAIL}$ **then**
- 14: **return** (B_j, W_{j-1}) ▷ guards rule out cycles, Sec. 4.4
- 15: **end if**

- 16: **if** $t = \text{RE}$ **then**
- 17: **for** $e_{str} \in \{\text{head}, \text{tail}\}$ with $4 < |e_{str}| < 60$ **do**
- 18: PROPAGATE($e_{str}, w_{cross_task_re}, \tau$) ▷ RE → NER, Sec. 4.4
- 19: **end for**
- 20: **else if** $t = \text{QAR}$ **then**
- 21: **for** $e_{str} \in \text{split}(\text{answer}, ", ")$ **do**
- 22: PROPAGATE($e_{str}, w_{cross_task_qa}, \tau$) ▷ QAR → NER, Sec. 4.4
- 23: **end for**
- 24: **else if** $t = \text{NER}$ **then**
- 25: $P \leftarrow P \cup \{\sigma\}$ ▷ NER → RE preemption set, Sec. 4.4
- 26: **end if**

- 27: **return** (B_j, W_{j-1})

- 28: **procedure** PROPAGATE(e_{str}, w, τ) ▷ graded cross-task update, Sec. 4.4
- 29: **if** $e_{str} \in W_{j-1}^{\text{NER}}$ **or** $\kappa(e_{str}) \geq 3$ **or** $B_j(e_{str}, \text{NER}) \geq 0.55$ **then**
- 30: **return** ▷ whitelist, cap, and severity-zone guards
- 31: **end if**
- 32: $s_{\text{before}} \leftarrow B_j(e_{str}, \text{NER})$
- 33: recurse: $U(e_{str}, \text{NER}, \text{SOFT_DOWNGRADE}, \tau, w)$ with $is_cross_task = \text{TRUE}$
- 34: $\Delta \leftarrow B_j(e_{str}, \text{NER}) - s_{\text{before}}$
- 35: $B_j(e_{str}, \text{NER}) \leftarrow s_{\text{before}} + \frac{1}{2}\Delta$ ▷ half-weight propagation
- 36: $\kappa(e_{str}) \leftarrow \kappa(e_{str}) + 1$
- 37: **end procedure**

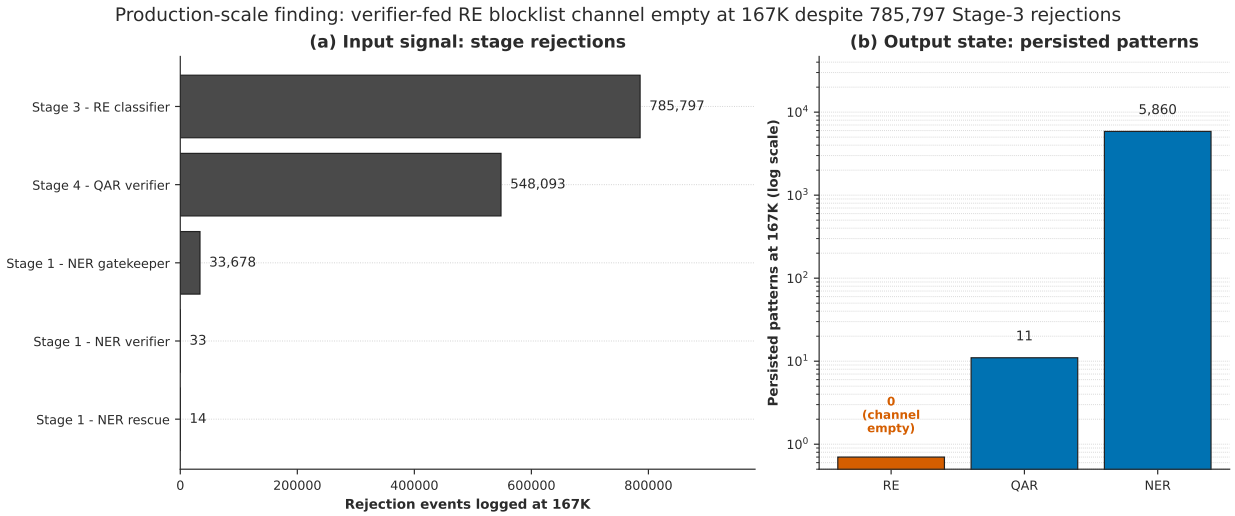


Figure 2: The verifier-fed relation-extraction persistence channel at 167,034-patient deployment scale. **(a)** Input signal: 1.37M rejection events logged across the five verifier stages, dominated by Stage 3 (relation classifier, 785,797 events, reason *SOTA_Classify_None*) and Stage 4 (QA verifier, 548,093 events). **(b)** Output state: persisted patterns at threshold in the relation, QA, and named-entity channels after the run (log scale). The relation channel is empty despite consuming 785,797 input events; the named-entity channel populates with 5,860 patterns and the QA channel with 11. This asymmetry is the central production-scale finding and motivates the verifier-independent Ontology-Violation Filter (Section 4.7).

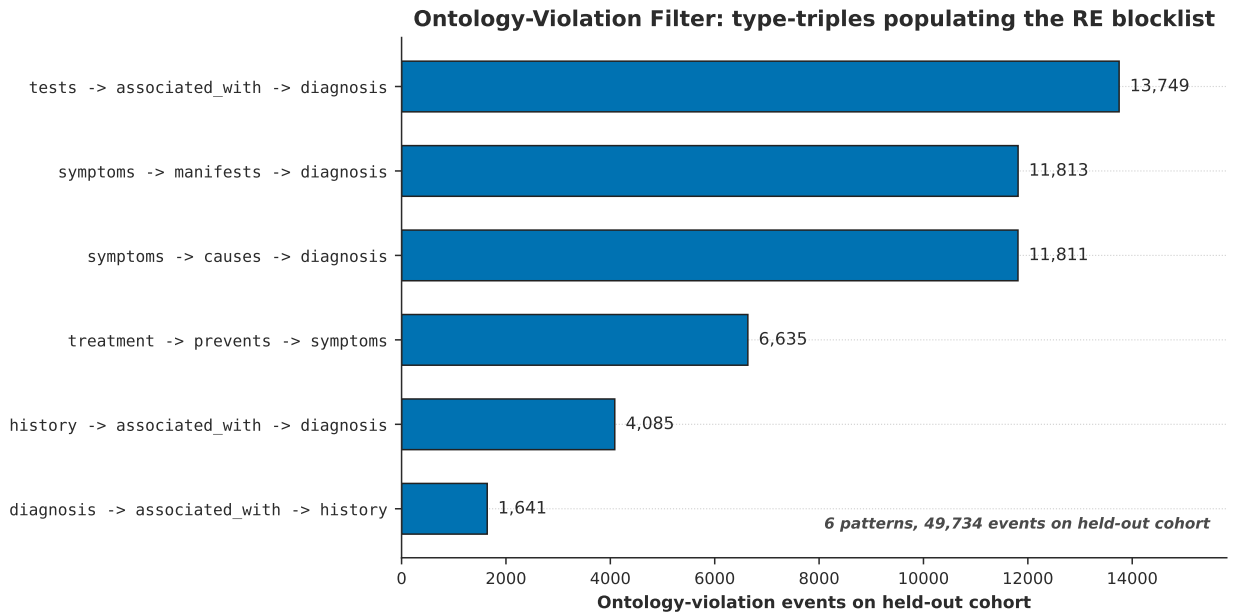


Figure 3: Type-triple patterns populating the relation blocklist through the Ontology-Violation Filter (Section 4.7) on the held-out cohort. Six threshold-clearing patterns aggregate 49,734 ontology-violation events. The Filter is a deterministic predicate (Equation 6) over head-type, relation, tail-type triples against a 29-entry clinical ontology, independent of the verifier-fed pathway whose collapse is documented in Figure 2.

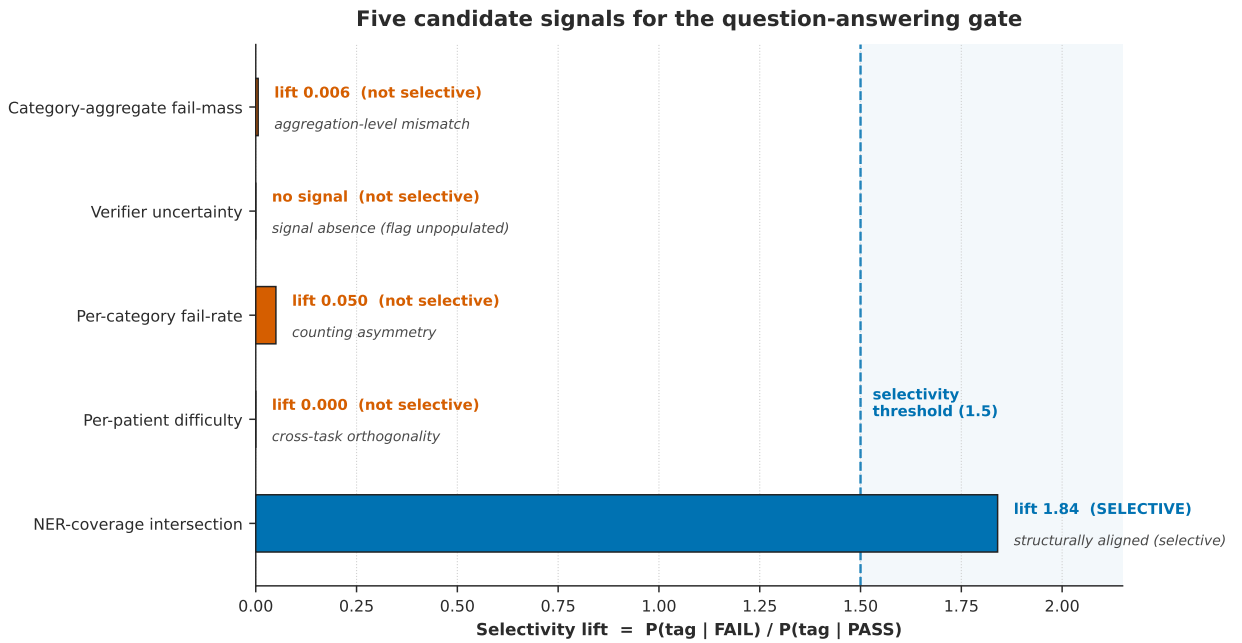


Figure 4: Selectivity lift of the five candidate signals for the question-answering gate on the held-out 5,000-patient cohort. Lift is defined in Equation (10) as $P(\text{tag} | \text{FAIL})/P(\text{tag} | \text{PASS})$; values ≥ 1.5 (dashed line) indicate selectivity. Four of the five signals fall below the threshold, each for the distinct reason labelled; the NER-coverage signal reaches a path lift of 1.84 in the full-DBPM configuration, within the 1.52–1.84 empirical band across four independent replications (Section 8.3).

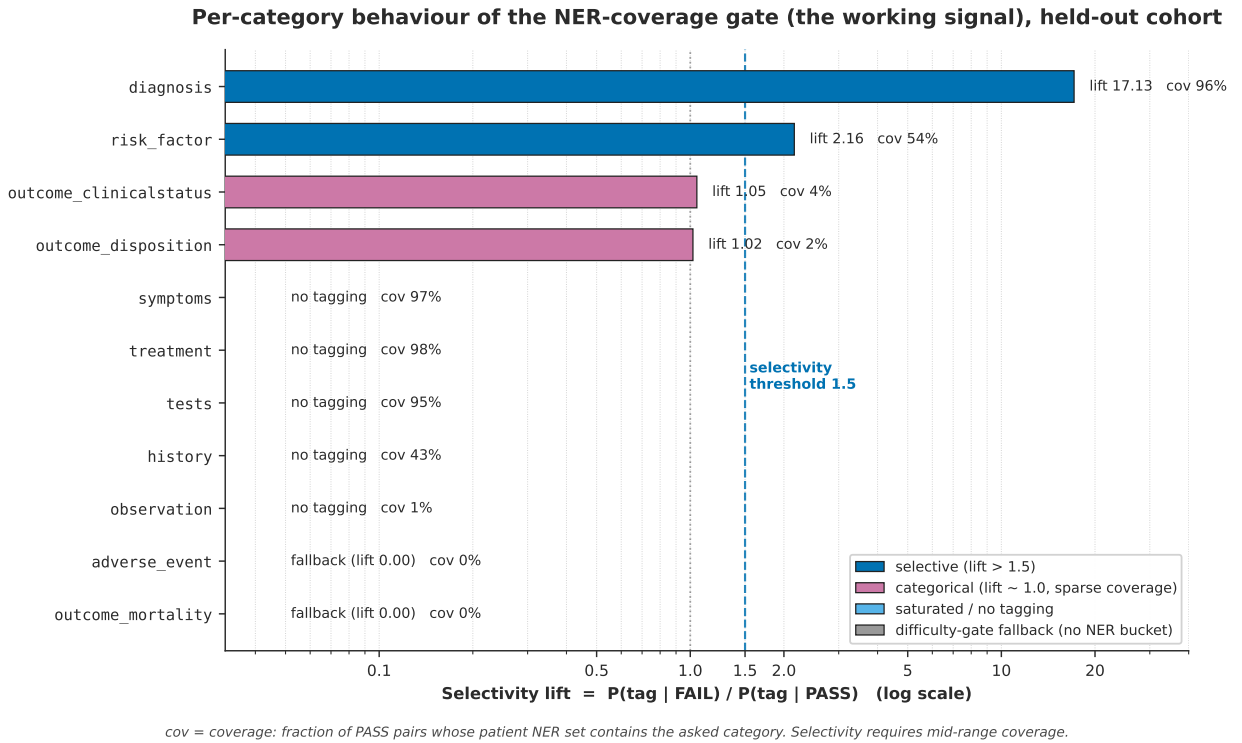


Figure 5: Per-category behaviour of the NER-coverage gate on the held-out cohort, the working signal of Section 6.3. Bars give the selectivity lift per QAR category on a log scale; coverage (the fraction of PASS pairs whose patient-level NER set contains the asked category) is annotated on each. The categories fall into four regimes: selective (*diagnosis* 17.13, *risk_factor* 2.16, both above the 1.5 threshold); categorical at sparse coverage (*outcome_clinicalstatus* 1.05, *outcome_disposition* 1.02); saturated or no-tagging at high or very low coverage (five categories); and difficulty-gate fallback where no NER bucket exists (*adverse_event*, *outcome_mortality*). Selectivity requires mid-range coverage: *diagnosis* is anti-selective in isolation but becomes the most selective category under full DBPM, as the Ontology-Violation Filter removes ontology-violating relations that inflate its coverage signal (Section 6.3).

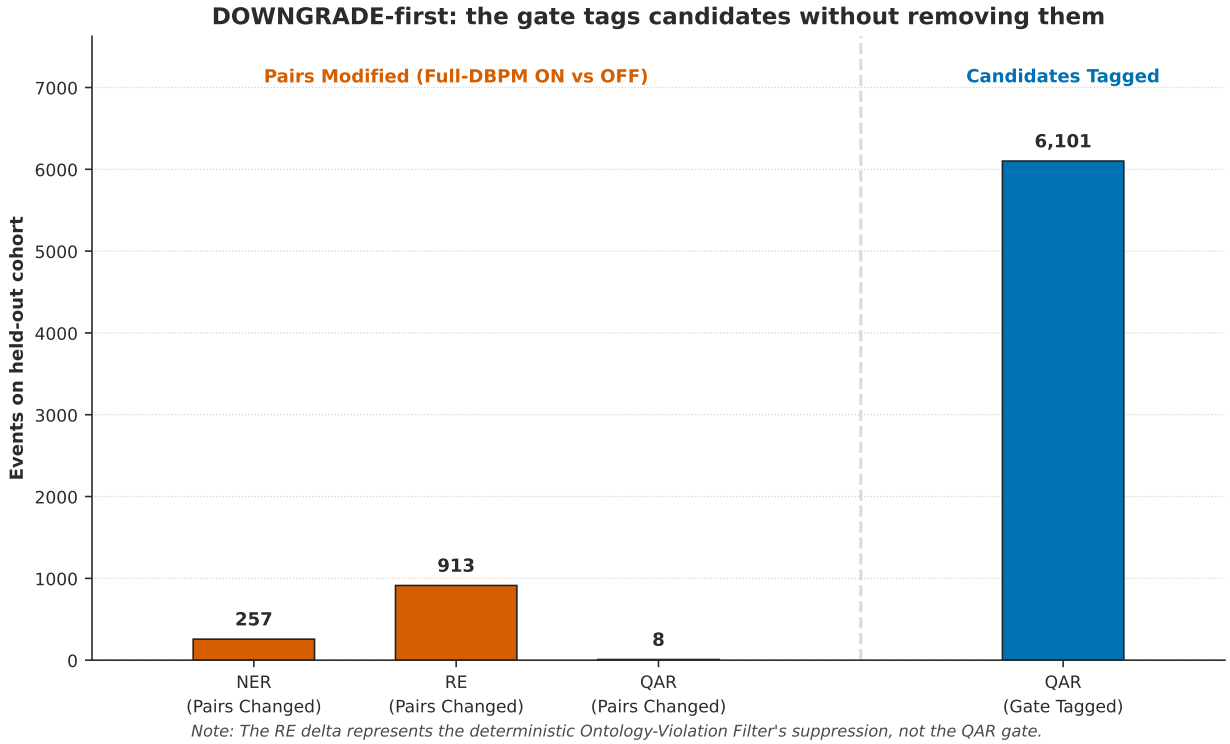


Figure 6: Pair-count deltas (left) versus gate-tag counts (right) on the held-out cohort under the full-DBPM ablation. The named-entity and QA pair-count deltas are within run-to-run noise (+257 and -8), confirming the DOWNGRADE-first discipline: the gate tags QA candidates without removing them. The relation delta of -913 is the Ontology-Violation Filter's genuine suppression, not a gate effect. The gate tags 6,101 PASS-side and 1,392 FAIL-side QA pairs (7,493 total), establishing selectivity at the tagging level rather than through output-volume change.